PART 1

Knowledge of Soil Mechanics

Machu Picchu, Peru

Machu Picchu is located at the top of a mountain which was far from the main transportation route at the bottom of a valley. Therefore, it was not found by modern people for a long time. This important cultural heritage is currently endangered by slope instability.

Chapter 1

# Basic Principles in Soil Mechanics

Tomb of Li Yuanhao 李元昊

The Tangut people established their kingdom of Western Xia 西夏 in the present Ningxia 寧夏 Hui Autonomous Region, Northwest China. The first emperor, Li Yuanhao, started his reign in 1038 and his empire became prosperous with income from the silk road trading. His tomb near Yinchuan 銀川 City used to be covered by beautiful tile decoration.

The contents of this book are classified into three groups that concern

Elementary topics with a symbol of   🗁

Advanced topics designated by   📖
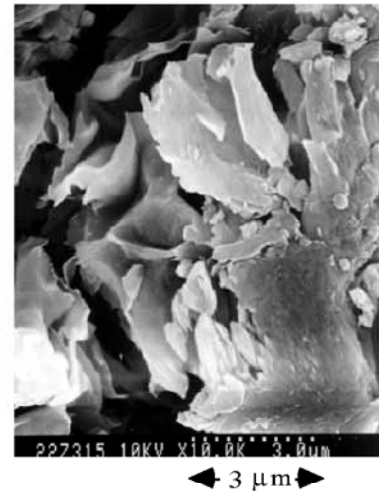
Miscellaneous topics accompanied by   💣※

Readers can choose sections that are important and relevant to their personal interests. They do not have to spend a long time by reading all the pages.

🗁   1.1 Physical Properties of Soil

Particle size is approximately 180 μm

1626 μm
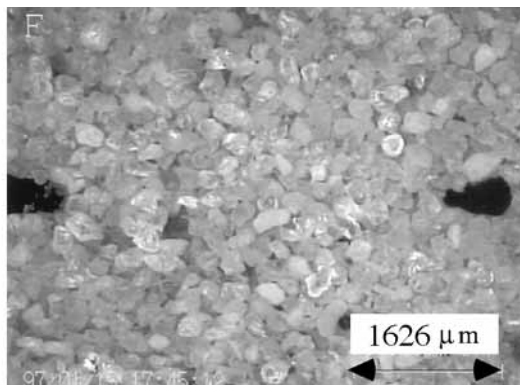
Fig. 1.1 Microscopic photograph of Toyoura sand

◀ 3 μm ▶

Fig. 1.2 Electronic microscopic photograph of bentonite clay (Towhata et al., 1993)

Soil is classified primarily into two categories; namely granular materials and cohesive soils. The former consists of gravel, sand, and cohesionless silts (Fig. 1.1), while the latter is clayey soil (Fig. 1.2). The mechanical properties of granular soils are governed by the grain-to-grain contact as well as friction. Hence, the magnitude of contact force and the geometrical nature of grain packing play major roles. It should be recalled that the magnitude of contact pressure per unit area of soil is called the effective stress, which is the most important concept in modern soil mechanics. In clayey soils, in contrast, chemical and electrical interactions among clay particles are important as well. Hence, shear strength is activated even at zero effective stress when the past stress–strain history allows it. Liquid limit (LL) and plastic limit (PL), which are called the Atterberg limits in combination, are two measures to evaluate the magnitudes of interparticle actions in addition to effective stress. The plasticity index, PI or I_p, is defined by PI=LL–PL. Generally speaking, PI of most clays lies in the range of 40–80 with such an exception of 400 or more of the sodium smectite (bentonite) group. As per 2006, the Japanese soil mechanic practice does not put " **%** " to the number of PI.

Another major difference between granular and cohesive soils lies in the grain size. The size affects the hydraulic conductivity (permeability or possibility of ground water to flow through soil). In conventional soil mechanics, grains larger than 75 μm are called
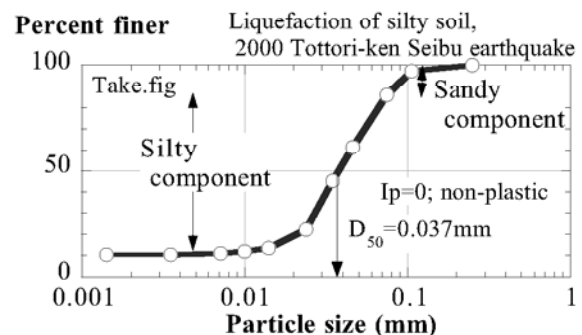
Fig. 1.3 Particle size distribution curve of silty liquefied soil

sand and those larger than 2,000 μm (2 mm) are gravel. On the other hand, particles smaller than 5 μm are clay in which chemical and electrical forces (cohesion) are important. Silt is a name of particles between 5 and 75 μm. Being called fine soils together with clay, silt has two groups. The first one is a plastic silt which includes clay minerals and has cohesion. The second group is nonplastic; being composed of small sand-like grains without cohesion. The difference of two silty soils should be borne in mind.

Figure 1.3 illustrates the particle size distribution of nonplastic silt, which liquefied during an earthquake (Sect. 17.10). The vertical coordinate denotes the accumulated (weight) percentage finer than the horizontal coordinate. Note that almost 80% of grains lies in the range of silt. The particle size at 50% is called the mean grain size, D_{50}. Hence, 50% of the total weight of soil is finer than D_{50}.

1.2 Weight and Density of Soil

The specific gravity, designated by G_s, stands for the mass density of minerals that compose grains divided by that of water. Hence, a unit volume of soil grain has a weight of $G_s\gamma_w$. Since most soil grains are made up similarly of silicate minerals, G_s of many soils, whether sandy or clayey, lies in the range of 2.6–2.75.

The weight of soil is important in calculating the earth pressure. When the weight of soil per unit volume, γ, is known, the overburden pressure (the vertical stress or the vertical compressional force per unit area) at the depth of z is given by $\sigma_z = \gamma z$. The range of γ is approximately around 15 (kN/m³) when soil is dry, and is 19–20 (kN/m³) or more under the ground water table. Soil is called water-saturated when the void space among solid particles is fully occupied by water, without air or gas bubbles. The extent of water-saturation is expressed by the degree of saturation, S_r. $S_r = 1.0$ (100%) when soil is fully saturated, and $S_r = 0.0$ when dry. Accordingly, the unit weight of soil is calculated by

$$\gamma = \frac{G_s\gamma_w + eS_r\gamma_w}{1+e}, \qquad (1.1)$$

where γ_w is the unit weight of water (9.8 kN/m³) and "e" is called void ratio, which is the ratio of open void volume among solid grains against the volume of solid phase, see Fig. 1.4. Moreover, the water content is defined by means of weight ratio;

Water content w

= ratio of weights of water and solid

$$= \frac{eS_r}{G_s}. \qquad (1.2)$$

In practice, soils under the ground water table is safely assumed to be 100 % saturated with water, $S_r = 1.0$ in (1.2).

Volume:			Weight:
$e(1-S_r)$	air		0
e	eS_r	water	$eS_r\gamma_w$
1		solid grains	$G_s\gamma_w$
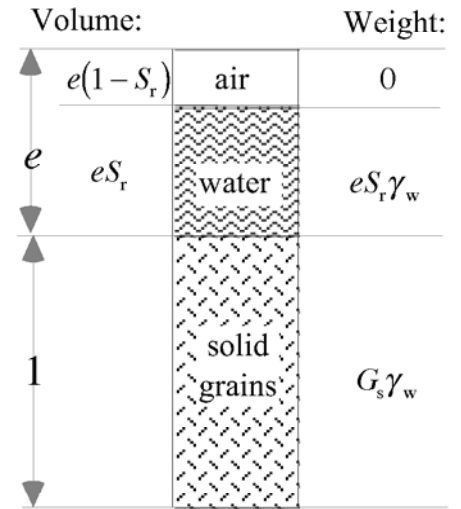
Fig. 1.4 Definition of void ratio

Section 1.3 will deal with the effective stress, which stands for the magnitude of contact force between soil grains. The effective stress plays an extremely important role in soil mechanics because the behavior of soil is strongly affected by grain-to-grain contact force. In contrast, the conventional kind of stress, which is the extent of force per unit area of soil and is referred to as the total stress, is less important. The overburden pressure as mentioned above is one of the total stresses.

The mechanical behavior and, for example, liquefaction resistance of sand are deeply affected by the state of granular packing. Denser packing improves the behavior of sand. This feature cannot be fully accounted for by void ratio (e) because the range of e taken by sand is varied by the grain shape and its surface roughness, and any sand is similarly weak at its maximum value of e. Therefore, a new parameter called the relative density (D_r) was introduced. $D_r = 0\%$ when sand is in the loosest state (void ratio $e = e_{max}$), and $D_r = 100\%$ when sand is in the densest state ($e = e_{min}$).

$$D_r = \frac{e_{max} - e}{e_{max} - e_{min}} \times 100(\%). \qquad (1.3)$$

Values of e_{max} and e_{min} are determined by several specified methods under zero overburden pressure. For example, soft sedimentation of dry sand or sedimentation in water is employed for the loosest grain packing (e_{max}) and continued shaking for the densest state (e_{min}). Note that states of loosest and densest packing change under higher pressures. $D_r = 0\%$ may be looser than the state of loosest packing under 100 kPa.

⌐ 1.3 Effective Stress and Pore Water Pressure

Sand at a depth of 100 m has greater shear rigidity and shear strength than the same type of sand at the ground surface. Although this difference may be partly due to density and geological history, its major cause is the strong contact forces between sand particles. Since the slipping at particle-to-particle contacts is a frictional phenomenon (Fig. 1.5), the greater contact force makes slippage difficult to occur, and increases the overall shear rigidity and strength. Thus, sand at a deep elevation is reinforced by the generation of high contact forces due to the weight of overlying soils.

N : contact force
S : frictional
    resistance
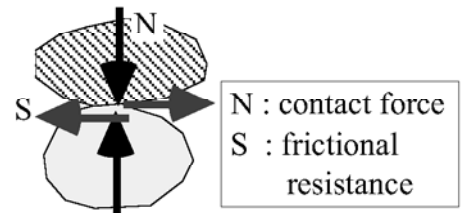
Fig. 1.5 Illustration of role played by intergranular contact force

The difference between the effective stress and the conventional (total) stress is found in the consideration of pore pressures. Pore pressure means the pressure of air and water in the pore (void among solid grains). When soil is saturated with water, pore air pressure is not of concern, and pore water pressure is designated by "u." Since pore water is one of the constituents of soil, the overburden pressure (vertical total stress) includes pore water pressure effects.

Pore water pressure does not affect the generation of frictional resistance at contact points as illustrated in Fig. 1.5. To understand this, compare the same sands, one is situated at the ground surface and the other upon the seabed at 10,000 m water depth. Clearly, the former has null total stress and the latter has 100 MPa. In spite of the high total stress, the seabed sand is soft due to null contact pressure. Note that pore water pressure at 10,000 m depth is 100 MPa, which is equal to the total vertical stress.

The idea of effective stress, σ', was introduced to understand the above discussion. With "′" as a symbol of effective stress,

$$\sigma' = \sigma - u. \tag{1.4}$$

For more information, refer to Fig. 18.2. At the seabed, therefore, the effective stress is

$$\sigma - u = 100\ MPa - 100\ MPa = 0\ MPa$$

and the behavior of seabed sand is similar to sand at the ground surface. Equation (1.4) is valid not only for the vertical stress but normal stresses in any directions. Shear stress in contrast does not have an idea of effective stress because pore water pressure does not have a shear component.
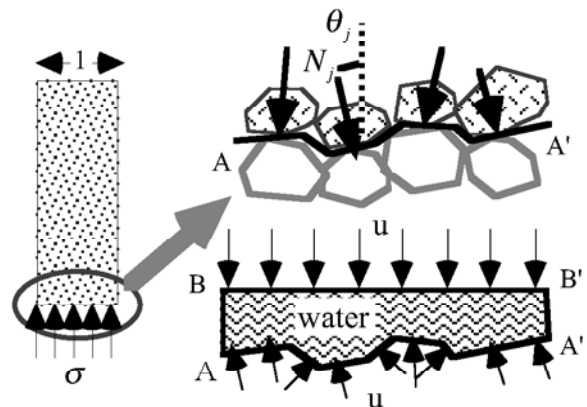
Fig. 1.6 Interpretation of physical meaning of effective stress

To understand the significance of effective stress, Figure 1.6 studies the force equilibrium of a soil column. The weight of the column with a unit cross section is equal to the total stress, σ. This is in equilibrium with the vertical components of pore water pressure, $\int_{A}^{A'} u \cos\theta\, ds$ and those of contact forces, $\sum_j N_j \cos\theta_j$ along AA', in which N_j is the magnitude of contact force and θ as well as θ_j is the direction. The summation and integration are made along AA', which is a curved bottom of the soil column that passes through pores and the granular contact points but never goes into grains. Another

force equilibrium shows that the integration of pore water along AA' is equal to the pore pressure, u, in a planar top of BB' (AB and $A'B' \ll BB'=1$),

$$\sigma = u + \sum_j N_j \cos\theta_j. \qquad (1.5)$$

By comparing (1.4) and (1.5),

$$\sigma' = \sum_j N_j \cos\theta_j. \qquad (1.6)$$

Thus, effective stress means a summation of granular contact forces per unit area in the direction of interest.

In a two-dimensional space in Fig. 1.7, there are three total stress components, and among them the normal stress components of σ_x and σ_z have effective stress components, $\sigma_x' = \sigma_x - u$ and $\sigma_z' = \sigma_z - u$. Note that the stress difference or shear component is identical for both total and effective stresses,

$$\sigma_z - \sigma_x = \sigma_z' - \sigma_x'. \qquad (1.7)$$

For any given stress state, the nominal values of stress components, σ_x, σ_z, and τ_{xz}, vary with the choice of coordinate system (direction of x and z axes). In Fig. 1.7, normal stress is positive in compression and shear stress is positive when it is oriented in counterclockwise direction. After rotation of the coordinate system by an angle of θ in the counterclockwise direction from x–z to x′–z′ system, the values of new stress components are calculated by using the theory of Mohr stress circle (Fig. 1.8).
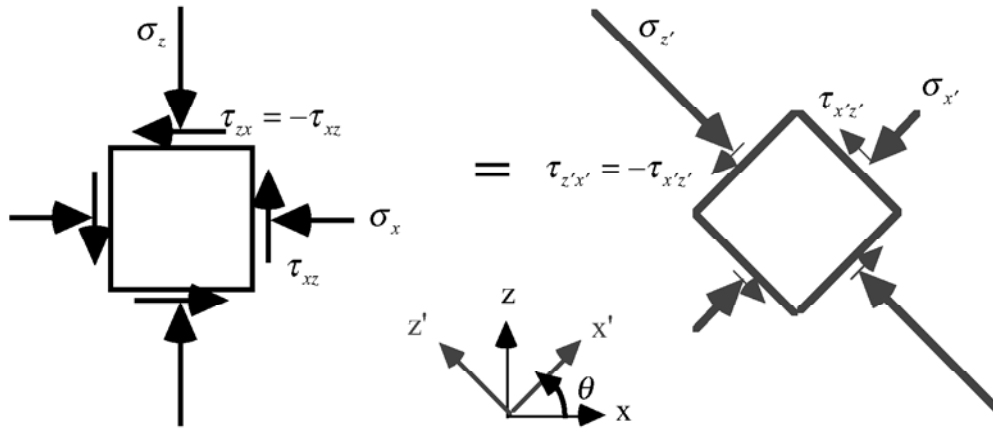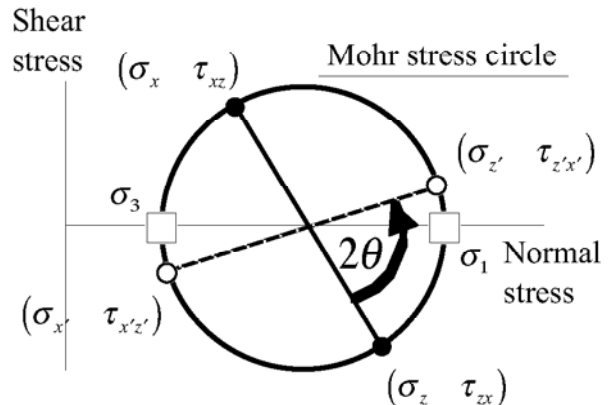

Fig. 1.7 Stress components undergoing rotation of coordinate system

By travelling along the Mohr stress circle in the counterclockwise direction by $2 \times \theta$,

$$\sigma_{x'} = \frac{\sigma_x + \sigma_z}{2} + \frac{\sigma_x - \sigma_z}{2}\cos 2\theta + \frac{\tau_{zx} - \tau_{xz}}{2}\sin 2\theta$$

$$\tau_{x'z'} = \frac{\sigma_x - \sigma_z}{2}\sin 2\theta + \frac{\tau_{zx} + \tau_{xz}}{2} - \frac{\tau_{zx} - \tau_{xz}}{2}\cos 2\theta$$

$$\tag{1.8}$$

$$\sigma_{z'} = \frac{\sigma_x + \sigma_z}{2} - \frac{\sigma_x - \sigma_z}{2}\cos 2\theta - \frac{\tau_{zx} - \tau_{xz}}{2}\sin 2\theta$$

$$\tau_{z'x'} = -\frac{\sigma_x - \sigma_z}{2}\sin 2\theta + \frac{\tau_{zx} + \tau_{xz}}{2} + \frac{\tau_{zx} - \tau_{xz}}{2}\cos 2\theta$$

Fig. 1.8 Conversion of stress components after rotation of coordinate axes

Equation (1.8) is further simplified because $\tau_{zx} = -\tau_{xz}$. It is important that the mean value of normal stresses is independent of coordinate rotation,

$$\frac{\sigma_x + \sigma_z}{2} = \frac{\sigma_{x'} + \sigma_{z'}}{2}. \qquad (1.9)$$

Figure 1.8 indicates that the stress circle crosses the horizontal axis at two points at which

$$\sigma = \frac{\sigma_x + \sigma_z}{2} \pm \sqrt{\left(\frac{\sigma_x - \sigma_z}{2}\right)^2 + \tau_{xz}^2}. \qquad (1.10)$$

Since these points have zero vertical coordinate, it is found that any stress states have two special planes, which have only normal stress components (1.10) and zero shear stress. These stress components are called principal stresses: major principal stress, σ_1, > minor principal stress, σ_3. The orientation of principal stress components are obtained by the geometric relationship in Fig. 1.8.

Direction of σ_1 plane is directed from the plane of σ_z at an angle of β in the counterclockwise direction;

$$\beta = -\frac{1}{2}\arctan\frac{2\tau_{zx}}{\sigma_z - \sigma_x}. \qquad (1.11)$$
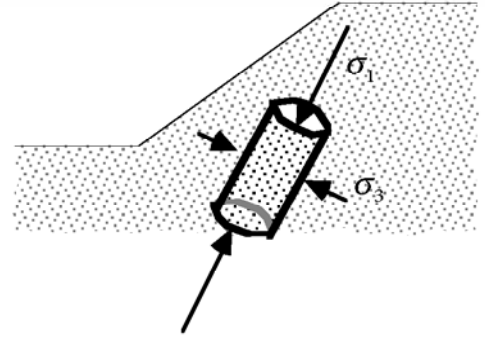
Fig. 1.9 Reproduction of field stress state in triaxial specimen

One of the important aims of unconfined and triaxial compression tests of soil mechanics is to reproduce the principal stress states in a cylindrical soil specimens and measure the deformation, which is equivalent to the field condition (Fig. 1.9). Note moreover that the above discussion concerning total stress is exactly valid for effective stress components as well.
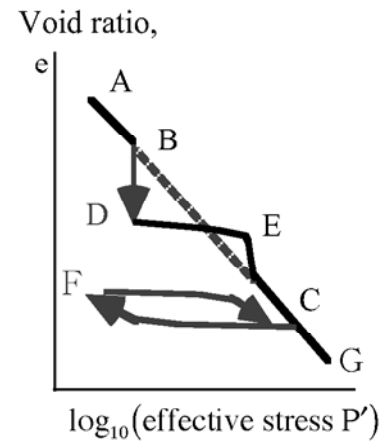
🗁 1.4 Consideration and Volume Change

Volume of soil varies with the effective stress. More accurately, the size of space (called void or pore) among solid grains decreases when the grain-to-grain contact forces increase. This is called primary consolidation. When the increment of effective stress, $\Delta P'$, is small, there is a proportionality between $\Delta P'$ and the volumetric strain of soil, $\Delta\varepsilon_{vol}$,

$$\Delta\varepsilon_{vol} = m_v \Delta P', \qquad (1.12)$$

where m_v is called the volume compressibility of soil. The subsidence induced by consolidation has long been a problem in soft clayey deposits subjected to surcharge or pumping of water. Both kinds of human activity increases the effective stress and induces the ground subsidence.

Void ratio, e

$\log_{10}$ (effective stress P′)

Fig. 1.10 So called "$e - \log P$" diagram on consolidation of soil

Terzaghi's classic theory of consolidation hypothesized that the volume change of soil is proportional to the increase of the vertical effective stress. More precisely, however, linear proportionality is not true. A semilogarithmically linear relationship as AG in Fig. 1.10 is often used in practice.

1. When consolidation starts from a state of slurry (mud) and the effective stress, P', increases continuously, the state of soil follows a linear path, ABCG, in Fig. 1.10. Soil in this process is called normally consolidated; the current stress is the highest as so far experienced. This is the case in alluvial plane where sedimentation occurs continuously.
2. The diagram in Fig. 1.10 should be called "e–logP′ diagram" but conventionally called e–logP diagram. Anyway, the horizontal coordinate stands for either the effective vertical stress or the mean of three effective stresses in orthogonal directions (effective mean principal stress).
3. When the effective stress is held constant at B, the process of secondary compression occurs and the volume decreases with time. Then loading resumes at D and the clay follows the path of DEC. Until E, the volume change is relatively small; after yielding at E, soil becomes normally consolidated. It is often the case that the point E lies above the normal consolidation line (AG).
4. Decrease of stress on CF is called unloading. The void ratio (or soil volume) does not come back to the original level at A. Thus, deformation of soil is irreversible. Then, the reloading from F back towards C follows a path similar to CF; after C, normal consolidation starts again towards G.
5. Soil in CFC is called overconsolidated. Overconsolidated soil is thus characterized by minor volume change upon loading, The overconsolidation ratio is defined by

$$OCR \equiv \left(\text{Ever highest effective stress}\right)/\left(\text{Present effective stress}\right) = \frac{P'_{\text{at C}}}{P'}.$$

6. The resemblance of DEC curve and FCG is noteworthy; significant volume contraction starts after an intermediate point. Note that this nature is induced by different mechanisms. Secondary compression or ageing (volume contraction under constant stress in BD) results are less volume change in DE, and the transfer of stress state from unloading (CF) / reloading (FC) to primary compression (CG) is important in FCG.

Primary consolidation is generated by compression of grain structure of soil due to change of effective stress. Little is known about secondary compression in contrast. Figure 1.11 shows that secondary compression in clay was accelerated by heating due possibly to thermal excitation of H_2O molecules that are electrically absorbed on surface of clay mineral.
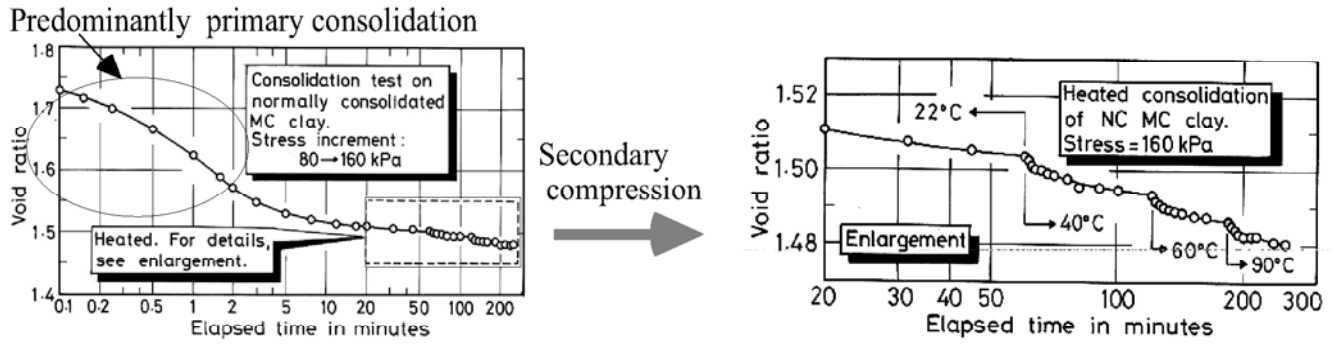
Fig. 1.11 Acceleration of secondary compression by heating of clay (Towhata et al. 1993)

The time required for the completion of consolidation settlement (completion of primary consolidation) is always important in practice. In principle, the consolidation time is governed by the amount of water that is drained out of ground (volume compressibility, m_v), the thickness of soil deposit (more precisely, the length of water drainage, H), and the easiness of water flow through clay (permeability, k, in Sec. 1.13). As illustrated in Fig. 1.12, the thickness of H stands for the length of water drainage. Many students, however, confuses this H with the thickness of clay deposits. When water is drained in both upward and downward directions due to good pervious layer at the bottom, H is half of the clay thickness.

Figure 1.13 illustrates the results of Terzaghi´s consolidation theory for a situation in which the ground surface is loaded by ΔP at time = 0. The nondimensional time (T) and the degree of consolidation (U) are defined by

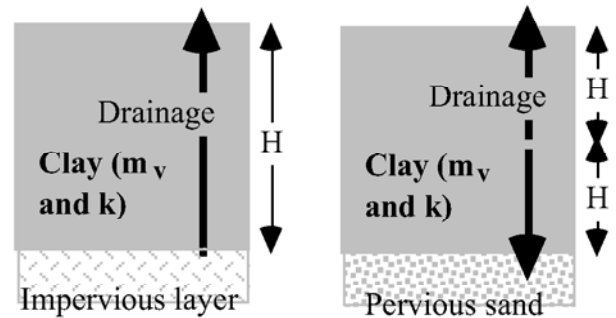$$T = \frac{\left(k / m_v \gamma_w\right) \times \text{time}}{H^2} \text{ and}$$

U = subsidence/ultimate subsidence,   (1.13)

respectively, and γ_w = 9.8 kN/m³ stands for the unit weight of water. Note that the ultimate subsidence is given by $m_v \Delta P \times$(thickness of soil). As mentioned before, this thickness of soil may be different from the drainage distance (H). The curve in Fig. 1.13 never comes to U=100%. In practice, therefore, the time for 90% consolidation (U=90%) is frequently referred to as an idea of time which is needed for consolidation
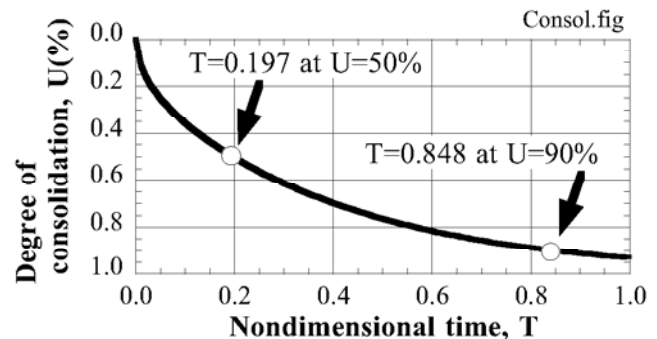

Fig. 1.12 Drainage of water from subsoil and consequent consolidation settlement

T=0.848 and
Time needed for 90% consolidation

$$= 0.848 \times \frac{H^2}{k / m_v \gamma_w}.$$ (1.14)

Fig. 1.13 Terzaghi´s theoretical progress of consolidation settlement

Thus, the consolidation time increases in proportion to H^2. For shortening of consolidation time, it is essential to make the drainage length as short as possible.

📁 1.5 Shear Deformation and Strength of Sand

The concept of "shear test" is understood by beginners more easily when a direct shear device is quoted than when a popular triaxial apparatus is. Figure 1.14 illustrates this device in which a sand specimen is placed between two rigid containers. After applying the effective (confining) stress in the vertical direction, the containers are forced to move laterally so that shear distortion occurs in the specimen. The shear stress is normally obtained by dividing the shear force by the cross section of the specimen. Since the strain in the specimen is not uniform, the extent of shear deformation is represented by the shear displacement. The vertical displacement of the upper container stands for the volume change of sand during shear (dilatancy).
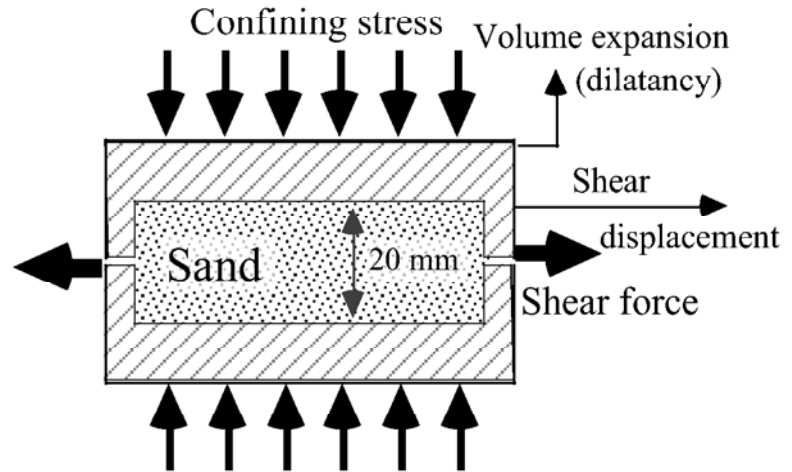
Fig. 1.14 Direct shear test

Figure 1.15 shows the relationship between shear stress and shear displacement. In the course of shear, the confining stress was maintained constant. This manner of test is called drained shear in soil mechanics because the volume of the specimen changes and causes flow (drainage) of pore water if sand is saturated with water. This figure demonstrates first that the stress-deformation relationship is not linear. Thus, the idea of linear elasticity has a limited significance in soil. Second, the peak shear stress increases with the effective stress. Thus, the shear strength of sand is interpreted by a frictional view point. Coulomb´s failure criterion states

$$\text{Shear strength} = \text{Effective stress} \times \tan\phi \qquad (\text{: Coulomb´s failure criterion}), \qquad (1.15)$$

where $\tan\phi$ stands for the frictional coefficient and ϕ is called the angle of internal friction. The slope of the curves stands for the shear rigidity of sand and increases with the confining stress. The stress level after large shear displacement is called the residual strength.

Figure 1.16 compares the stress–displacement behavior of medium dense sand (relative density=55%) and very loose sand ($D_r = 0\%$). Note that the peak strength of loose sand is much lower, while the residual strength is similar.
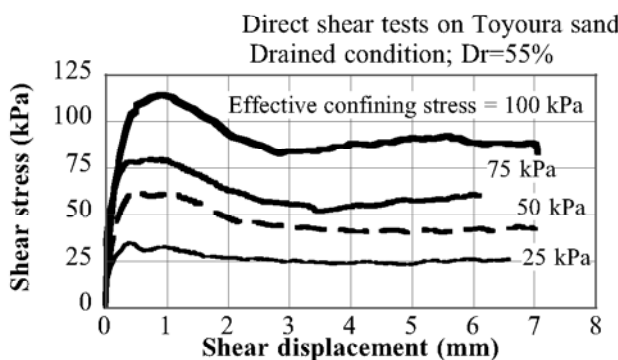
Fig. 1.15 Effects of confining stress level on drained stress–strain behavior of sand
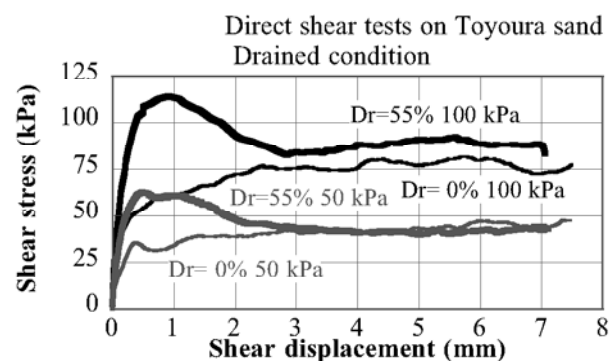
Fig. 1.16 Effects of density of sand on drained stress–strain behavior of sand
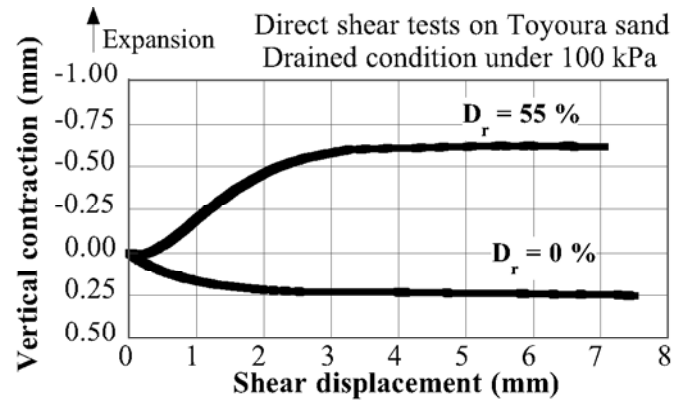
1.6 Dilatancy or Shear-Induced Volume Change

Figure 1.17 shows the relationship between shear displacement and vertical displacement (= volume expansion/contraction) during direct shear tests. Since the height of the sand sample was 20 mm at the beginning of shear, the 1 mm displacement stands for 5% expansive strain.
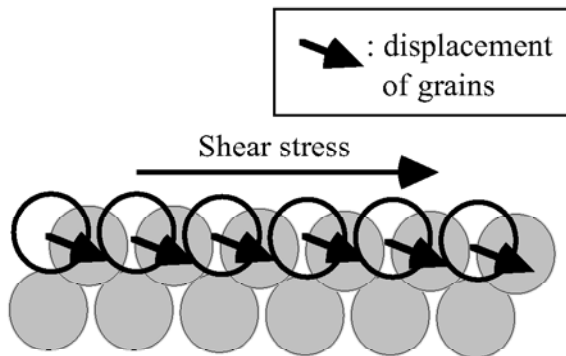
The shear-induced volume change occurs in a variety of materials. For example, concrete and rock develop cracking prior to failure, and the apparent overall volume increases.

Fig. 1.17 Volume change of sand during direct shear test

The earth crust sometimes develops cracking before rupture (earthquake) and creates such earthquake precursors as small earthquakes and change of deep ground water level as well as chemical composition of water. For these materials, the volume increases and this behavior is called "dilatancy."
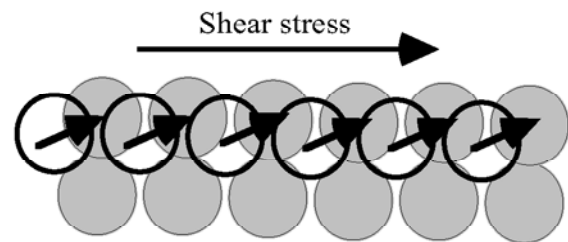
In case of sandy materials, volume increases or decreases according to loading conditions. For example, Fig. 1.17 shows that the volume of medium dense sand (55% relative density) increases (dilatancy), while the volume decreases (contraction or negative dilatancy) for very loose sand.
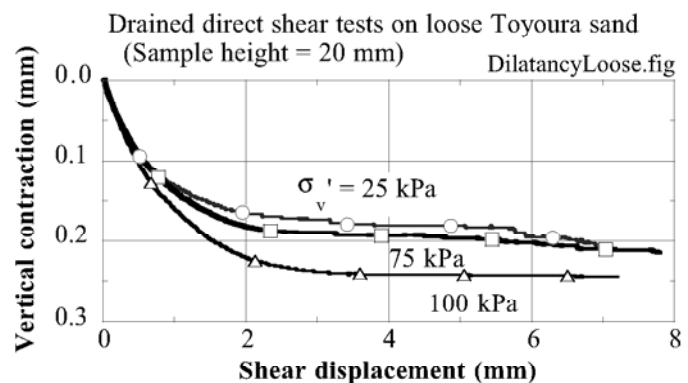
Fig. 1.18 Dilatancy of loose sand

Fig. 1.19 Dilatancy of dense sand

The mechanism of dilatancy is illustrated in Figs. 1.18 and 1.19. When sand is loose (Fig. 1.18), the loading of shear force on sandy grains makes grains fall into large voids. Thus, the apparent height of the sandy deposit decreases. On the contrary, when sand is dense (Fig. 1.19), grains climb up adjacent grains. Thus, the overall volume increases. Note that this effect of density on nature of dilatancy is superimposed by the effect of confining stress; the volume expansion of dense sand under

Fig. 1.20 Effects of stress level on extent of dilatancy

low effective stress may change to volume contraction under higher stress. Thus, Fig. 1.20 illustrates that loose sand under 100 kPa is more contractive than the same sand under 25 kPa. Bishop (1950) discussed the effects of dilatancy on shear strength of sand, and Rowe (1962) proposed the idea of stress–dilatancy relationship for deformation theory of sandy soils

$$\frac{\tau}{\sigma'} = K\left(-\frac{d\varepsilon_v}{d\gamma}\right) + \text{constant}, \qquad (1.16)$$

in which τ and σ' are shear and effective normal stress, respectively, γ and ε_v are shear and volumetric (positive in contraction) strains, and K is a constant parameter. The nature of this equation is illustrated in Fig. 1.21.
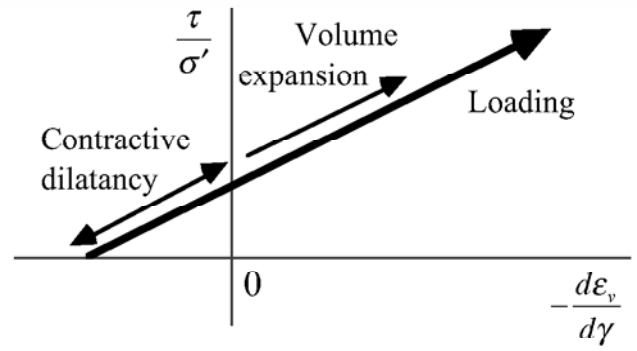
Fig. 1.21 Schematic illustration of stress–dilatancy equation

🗁 1.7 Undrained or Constant-Volume Shear Test

The shear tests as stated in Sects. 1.6 and 1.7 were subjected to volume change of sand. When tested sand is saturated with water (S_r=1.0), this volume change is associated with migration of pore water into or out of sand. The direction of water migration depends upon the nature of dilatancy. Water flows into sand when sand is dense and dilatancy is positive (volume increase), while water comes out of sand when sand is loose and dilatancy is negative (volume contraction). Anyhow, shear associated with water migration is called drained shear.

Since real alluvial ground in general has the thickness of meters or more, water migration and drainage take time to occur. Even in sandy ground in which the permeability coefficient is high, the needed time is often of the order of tens of minutes. Since this time is much longer than the earthquake duration time, it is reasonable that seismic loading on real ground, whether it is sandy or clayey, is associated with a negligible extent of drainage. In engineering practice, therefore, it is considered that no drainage occurs in sandy ground during seismic shaking. This situation is called undrained loading. When soil is fully saturated with water (S_r=1.0), volume of soil does not change during undrained loading.

It is very important that volume change of soil during drained loading is converted to change of pore water pressure during undrained shear of water-saturated soil, and finally the rigidity and shear strength of soil are significantly affected. Figure 1.22 illustrates this mechanism. Figure 1.22a shows a drained condition in which a piston is pushed into a cylinder and water in it is easily drained out of a hole. In this situation the pressure of water in the cylinder does not change very much. In contrast when the drainage hole is closed in Fig. 1.22b, water cannot get out of the cylinder although the piston is pushed. Consequently, the pressure increases in the water and achieves equilibrium with the external force. Thus, volume contraction in loose sand undergoing drained shear is equivalent with pore water pressure increase in loose sand subjected to undrained shear. Similarly, the volume increase (positive dilatancy) in denser sand during drained shear is equivalent with pore pressure decrease in undrained shear.

Undrained shear is otherwise called constant-volume shear. Note that the effective stress principle of soil mechanics, (1.4), implies that the increase of pore water pressure (u) in loose sand results in reduced effective stress (σ') if the total stress (σ) is held constant.

(a) Drained condition   (b) Undrained condition
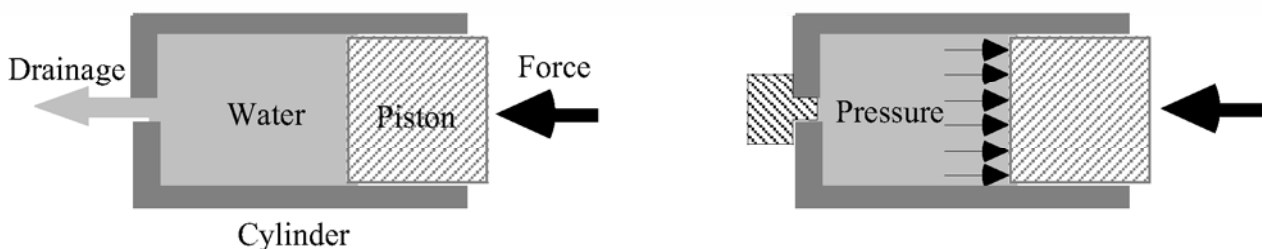

Fig. 1.22 Simple illustration of drained and undrained conditions

## 🗁 1.8 Excess Pore Water Pressure and Stress Path Diagram

Figure 1.23 illustrates the results of direct shear tests as mentioned in Sect. 1.5. Since some tests were carried out by maintaining constant the volume of specimen (height) , it was possible to examine the effects of drainage condition on the shear behavior of sand. It is therein seen that the stress–displacement behaviors in drained and undrained tests are completely different. Moreover, the denser sand (D_r=55%) has the greater rigidity and strength in undrained shear than in drained shear, while conversely the loose sand (D_r=0%) has much lower strength during undrained shear. This difference was induced by the change of the effective stress.

Figure 1.24 shows the relationship between the effective stress and shear stress for two values of relative density (0% and 55%). A diagram of this type is called "stress path" and plays a very important role in interpretation of undrained behavior of soils. It is seen in this figure that the effective stress of denser sand increased drastically after a minor decrease. This increased stress level resulted in the greater stiffness and shear strength as seen in Fig. 1.23. In contrast, the effective stress in loose sand (D_r=0%) was reduced significantly and as a consequence the sand became very soft.

In soil mechanics, the change of effective stress is often induced by the change of pore water pressure (see (1.4)). The change of pore water pressure from its initial value is called excess pore water pressure.
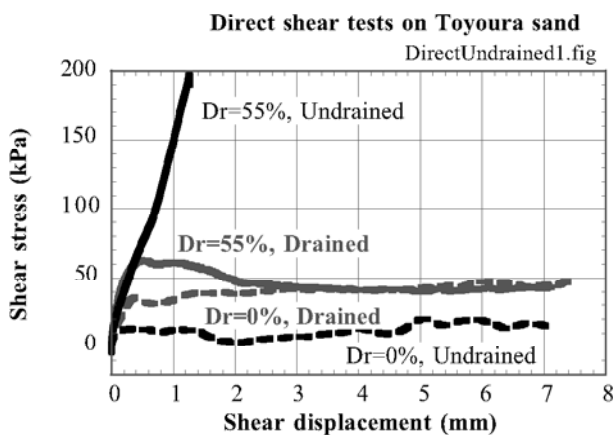
Fig. 1.23 Effects of drainage condition on stress-displacement relationship of sand
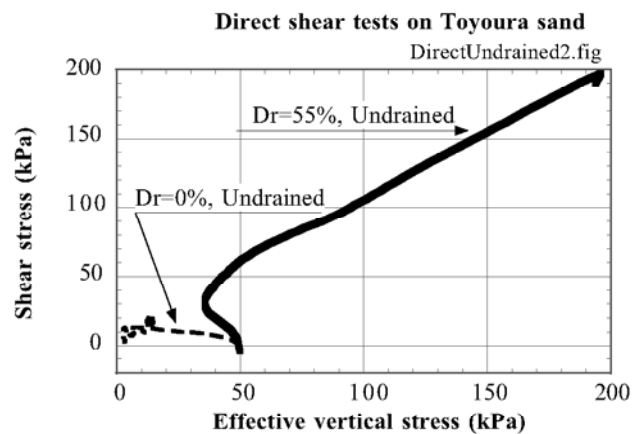
**Fig. 1.24** Stress path diagram for undrained shear tests

1.9 Triaxial Shear Device

Although the mechanical principle of direct shear in Sect. 1.5 is easy to understand, practical soil testing is more widely conducted by using a triaxial device. As illustrated in Fig. 1.25, a soil specimen of a columnar shape is covered by a rubber membrane, pressurized by equal pressure in both horizontal and vertical directions, and additional stress is loaded in the vertical direction. Although being called triaxial, this device controls only two stress components. The horizontal stress is often called the radial stress, σ'_r, and the vertical stress is called the axial stress, σ'_a.

Some people ask questions why the loading of axial stress is not compression but shear. An answer to this question may be found in Fig. 1.26 where failure of a sand specimen was caused by the loading of axial stress. A development of shear failure along an inclined plane is evident.

The triaxial apparatus is more popular than a direct shear device or a similar simple shear machine because the cylindrical shape of a triaxial apparatus makes it easy to run tests on samples of a good quality collected from the site (undisturbed specimen which preserves the nature of soil in the field).

Figure 1.27 illustrates a schematic result of triaxial shear test in which the radial stress is held constant and the axial stress is increased. Note that shear deformation and failure are induced by the difference of σ'_a and σ'_r. Hence, the deviator stress of $\sigma'_a - \sigma'_r$ plays a major role. The volume change of the sample is measured by using a burette that monitors the volume of pore water that comes out of the sample. To do this, the sample has to be saturated with water.
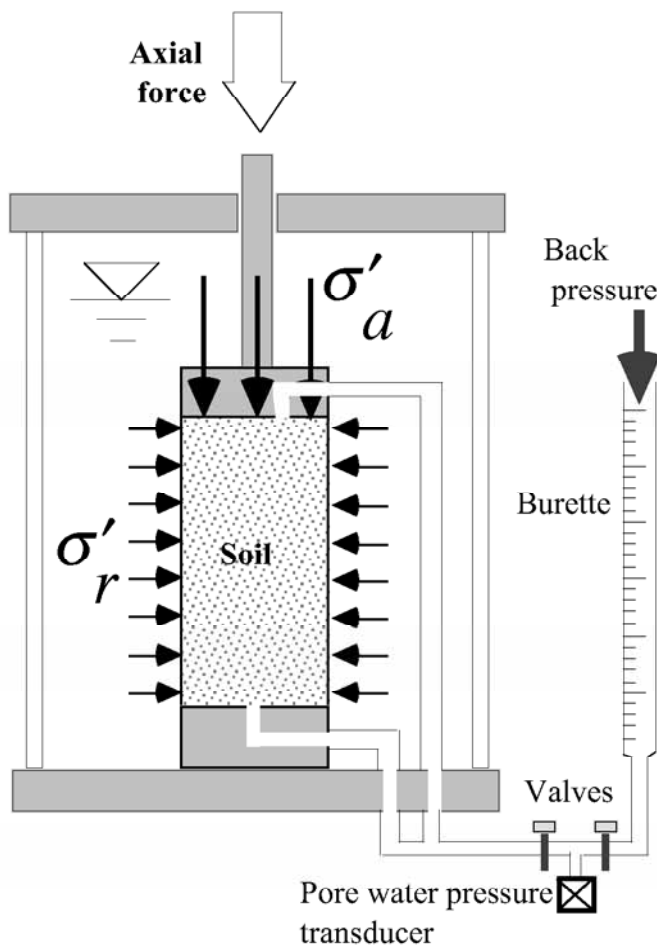

Fig. 1.25 Stress condition in triaxial soil specimen

Fig. 1.26 Development of shear failure due to loading of axial stress (Photo by M.Mizuhashi)

There are many variations in triaxial tests.

- Undrained tests (Sect. 1.7) are run by closing the right valve in Fig. 1.25. In place of volume change, pore water in the sample varies with shear deformation.
- Triaxial extension tests are run by either increasing σ_r' or decreasing σ_a' by which the sample is elongated in the axial direction.
- Strain-controlled tests are carried out by controlling the velocity of axial displacement. Upon softening after the peak stress (see Fig. 1.27), strain-controlled tests can follow the decreasing stress level. Note that this capability is achieved when the rigidity of the loading device is substantially greater than that of a specimen. Thus, a soil testing machine can record softening behavior of soft clay or liquefied sand. However, the same machine cannot record softening of hard rock or concrete.
- Stress-controlled tests are conducted by controlling the magnitude of the axial stress. Since the stress is directly applied by supplying air pressure into a belofram cylinder, the decrease in the stress level as in Fig. 1.27 cannot be recorded. In place of softening of stress, stress-controlled tests suddenly develop very large strain (Fig. 1.28).
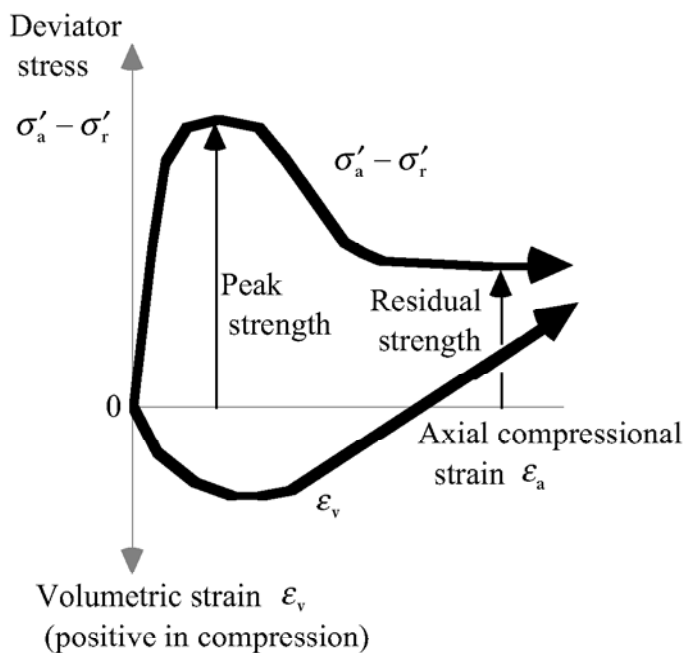
Fig. 1.27 Schematic idea of stress≷strain behavior of soil in triaxial compression test
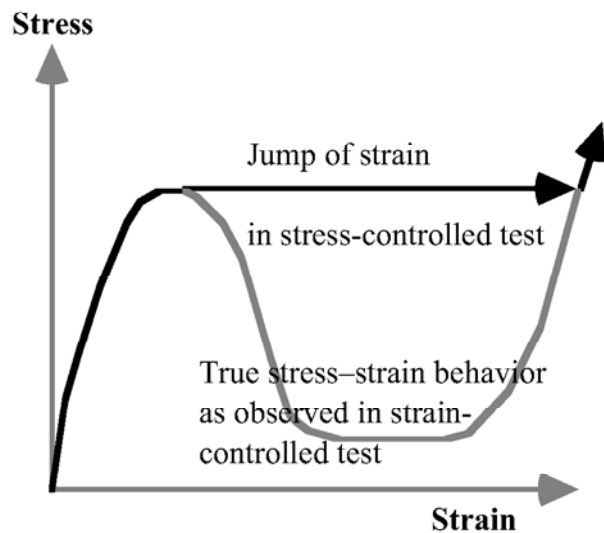
Fig.1.28 Missing stress softening behavior in stress-controlled tests

✸ 1.10 Membrane Penetration

The problem of membrane penetration, which is otherwise called membrane compliance, is important in undrained shear tests on coarse granular materials. Figures 1.29 and 1.30 show triaxial specimens of Chiba gravel undergoing negative pore pressures of –1 kPa and –10 kPa, respectively. It is clearly seen that the increase of the negative pressure from –1 to –10 kPa made the rubber membrane move into voids. This phenomenon is very significant in the illustrated case because the thickness of the employed membrane (approximately 0.25 mm) is much thinner than the size of the gravel that ranges between 4.75 and 9.5 mm. Note that the inward movement of the membrane upon increase of negative pressure (increase of effective stress) causes additional change in void volume, which is not related with the volume contraction of granular structure of soil.
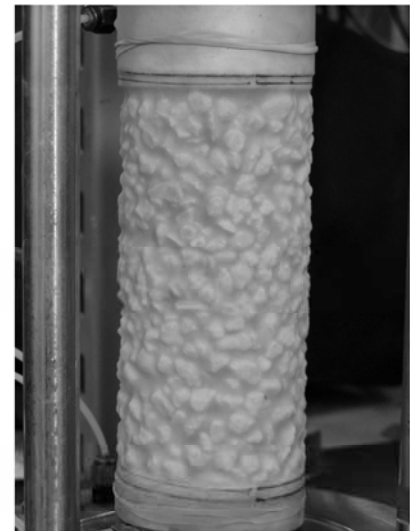
The membrane penetration problem is significant in liquefaction tests on coarse grained soils as well, because the development of excess pore water pressure and decrease of effective stress lead to the outward movement of membrane (from Fig. 1.30 to Fig. 1.29, see Fig. 1.31). Thus, pore water migrates outwards from a tested specimen. Since this migration is equivalent with drainage of pore water, the measured excess pore water pressure is an underestimation in the test and, consequently, liquefaction resistance is overestimated.

Many attempts have been made to make correction of the membrane-penetration errors by evaluating the magnitude of membrane migration during change of effective stress. Experimentally, it is interesting to push water into a specimen in order to compensate for the penetration-induced drainage.

In principle, the experimental error in undrained tests due to membrane penetration can be reduced by either physically reducing the extent of penetration or injecting pore water into a specimen by the same amount as membrane penetration. As for the former idea, use of thick membrane might cause another problem: error in stress condition due to tensile force in the membrane. In this account, Towhata et al. (1998) pasted pieces of thin metal plates between membrane and gravelly soil.

The amount of membrane penetration volume is a function of effective stress (difference between outer pressure and internal pore pressure). Thus, the penetration volume change has been experimentally evaluated by running a variety of drained tests. Newland and Allely (1957) assumed that difference between axial and radial strains during isotropic compression in triaxial tests is equal to the membrane penetration error. This idea, however, does not work because of anisotropic nature of sand. Roscoe (1970) and Raja and Sadasivan (1974) as well as Nicholson et al. (1993) embedded different volumes of brass rods and conducted isotropic compression. While the measured volume change varied with the amount of brass rods, the net

Fig. 1.29 Appearance of Chiba gravel specimen undergoing 1 kPa of effective stress

Fig. 1.30 Appearance of gravel specimen undergoing 10 kPa of effective stress

——— Membrane before pore pressure development
——— Membrane after pore pressure development
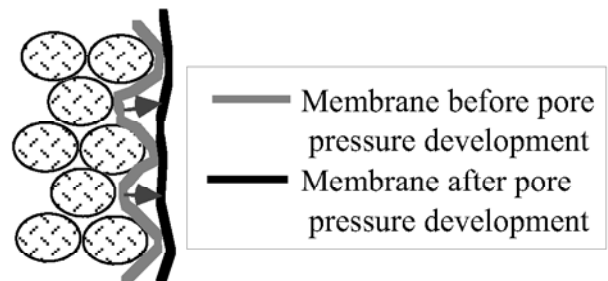
Fig. 1.31 Drainage induced by membrane penetration

volume change in sand was assumed constant. By extrapolating the volume change to 100% volume of brass, the membrane penetration was evaluated. It is not clear whether or not interaction between brass and sand affected volume change of sand. Evans et al. (1992) filled void among gravel particles with loose fine sand, thus preventing penetration of membrane. Finally, Sivathayalan and Vaid (1998) proposed an idea for a hollow cylindrical specimen. In their idea, a hollow cylindrical specimen is subjected to drained isotropic consolidation, and a geometrical relationship in volumetric change of a tested specimen and the internal hollow space is used to assess the extent of membrane penetration as a function of effective stress. It is important for readers to fully understand the derivation of their equation prior to using it.

🗀 1.11 Elementary Dynamics

Basic knowledge on theory of vibration is very important in understanding ground response to earthquake excitation. Figure 1.32 illustrates a single-degree-of-freedom model in which a mass of m is subjected to oscillatory force of $F(t)$. The mass is connected to a fixed support by means of a linear elastic spring of k. By denoting the displacement of the mass by u, the equation of motion of this system is derived as

$$m\frac{d^2u}{dt^2} + ku = F(t), \qquad (1.17)$$

in which t stands for time.

When $F(t)$ is a sinusoidal function of time, $F = F_0 \sin\omega t$, the solution of u is given by

$$u(t) = \frac{F_0}{k - m\omega^2}\sin\omega t. \qquad (1.18)$$

Fig. 1.32 Single-degree-of-freedom model

This implies that the mass in Fig. 1.32 oscillates by a sinusoidal function with a period, T, of $2\pi/\omega$. The frequency (number of cycles per second, f) is given by $f = 1/T$, while "ω" is called the circular frequency. Note that $\omega = 2\pi f$. The amplitude of the motion (1.18) changes with the shaking frequency (ω) as illustrated in Fig. 1.33. In particular, it becomes infinite when $\omega = \omega_n = \sqrt{k/m}$.

Fig. 1.33 Amplification curve for single-degree-of-freedom model

This significant magnitude of motion is called resonance. The period of the force, $T_n = \omega_n/(2\pi)$ is known as the natural period, while the frequency of $f_n = 1/T_n$ is the natural frequency. When any structure is subjected to external force, the situation of resonance has to be avoided.

The above discussion assumed that everything changes with a harmonic (sin) function of time. In reality, the motion starts at some time ($t=0$). When u = 1.0 and $du/dt = 0.0$ at time $t=0$ (initial conditions) under $F(t) = 0.0$, the solution of (1.17) is given by

$$u(t) = \cos\omega_n t. \qquad (1.19)$$

Thus, the motion without external force (free vibration) occurs with the natural period.

Moreover, the external force, $F(t)$, may start at $t=0$. Then, another solution under $F = F_0 \sin\omega_n t$ at a resonant frequency while $u = u(0)$ and $du/dt = 0$ at $t=0$ is derived

Fig. 1.34 Transient solution of motion under resonance frequency

$$u(t) = \frac{F_0}{2k}\left(\sin\omega_n t - \omega_n t \cos\omega_n t\right) + u(0)\cos\omega_n t. \qquad (1.20)$$

This implies that the amplitude of motion increases with time; see an example calculation in Fig. 1.34. This type of oscillation is called transient. Thus, the infinite amplitude of motion at resonance, as suggested by (1.18), takes infinite duration time of excitation to occur.
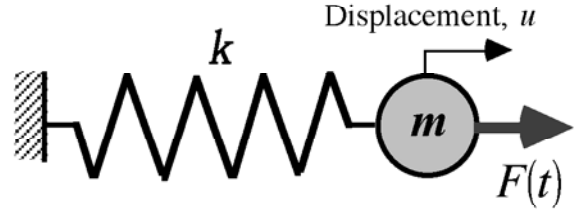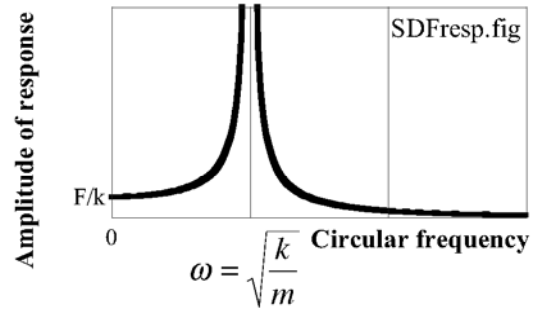
The soil investigation in the field aims at collecting information that helps to assess the mechanical properties of soils as well as stratification of the ground. On the other hand, such mechanical properties of soils as shear modulus and shear strength can be obtained by drilling a bore hole (boring), collecting soil samples of good quality, and running tests in the laboratory. However, this elaborate procedure is often more time consuming and expensive. Problem of sample disturbance error is another big issue. Thus, field tests that can be run in a bore hole is often preferred.

Standard penetration tests, which is abbreviated as SPT, have a long history (Fig. 1.35). A cylindrical tube of a specified size is penetrated into the bottom of a bore hole by repeating hammer impacts at the ground surface (Fig. 1.36). Since the mass of the hammer and the height of its free fall are specified as 63.5 kg and 76 cm, respectively, one blow produces impact energy of 0.467 kJ. With this specified energy, it is expected that the obtained results are of universal use. The number of hammer impacts (blows) is counted and the one which is needed to achieve 30 cm penetration is called SPT-N. This N value stands for the resistance of soil against penetration of a tube and most probably has a good correlation with shear modulus, shear strength, and density of soils.

The good points of SPT are as what follows:

– Equipment is mechanically simple
– Disturbed soil sample is collected by the penetrated tube (Fig. 1.37)
– Thus, types and physical properties of soils (Sect. 1.1) can be measured directly, although mechanical properties cannot be measured due to significant disturbance of soil
– There is a huge number of empirical correlations between SPT-N and mechanical properties of soils.

On the other hand, its shortcomings may be as what follows:
– State of maintenance of the equipment affects the measured N value
– The measured N value is affected by the effective stress in the ground, σ'_v, and does not represent the true nature of soil
– SPT-N is subjected to human errors such as insufficient height of free fall (<75 cm) and poor maintenance efforts
– The free-fall energy is not fully employed for penetration of the tube, making real impact energy to be, for example, 60–70 % of the ideal value of 0.467 kJ

Fig. 1.35 Practice of standard penetration test
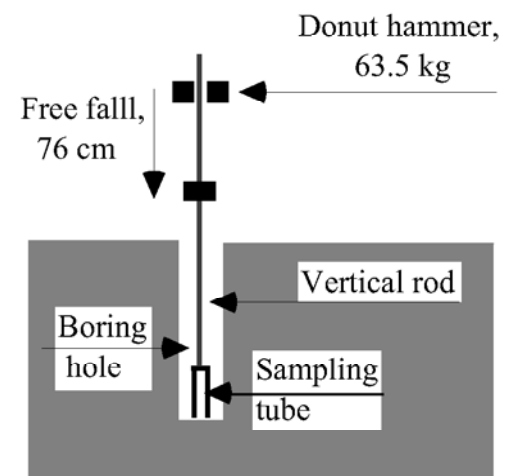
Fig. 1.36 Conceptual idea of standard penetration test

Fig. 1.37 Disturbed soil sample collected by tube

Seed et al. (1985) discussed the possible sources of errors in SPT such as insufficient impact energy,

length of rod, and type of tip sampler. In this regard, attempts have been made to solve the problem of insufficient height and accordingly the insufficient free-fall energy. An example of such an attempt is the automatic free-fall device (Fig. 1.38). This device, however, needs more human load and makes the field operation less efficient. Effort for maintenance of this equipment is another problem. Thus, the precise achievement of the required free-fall energy is not yet universally achieved. Consequently, it has been practiced to correct measured N value to the one at 60% of the specified energy under effective stress of 98 kN/m^2 (1 kgf/cm^2).

$$N_{1,60} = \frac{0.467 \times 0.6}{\text{Real impact energy}} \times \frac{1.7 \times (\text{Measured } N \text{ value})}{\sigma_v'\left(\text{kgf}/\text{cm}^2\right) + 0.7}. \tag{1.21}$$

Moreover, it should be noted that fines content in soil (particles finer than 75 μm) makes the measured N value smaller. Meyerhof (1957) proposed an empirical relationship between SPT-N and relative density of sand. Japanese Geotechnical Society (2004) employs its modification for sands with fines for design of soil improvement against liquefaction (Sect. 26.5);

$$D_r(\%) = 21\sqrt{\frac{N}{0.7 + \sigma_v'/98} + \frac{\Delta N_f}{1.7}}, \tag{1.22}$$

in which σ_v' is the effective vertical stress (kN/m^2) and ΔN_f stands for the correction for fines content (finer than 75 μm), see Fig. 1.39.

Fig. 1.38 Example of free-fall standard penetration equipment
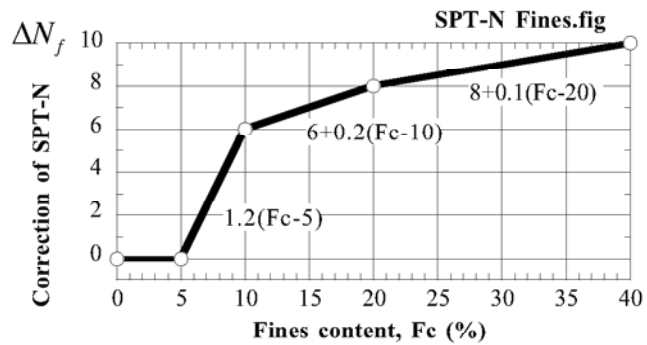
Fig. 1.39 Correction of SPT-N in terms of fines content (JGS, 2004)

⌂ 1.13 Flow of Ground Water

It may be thought that the flow of ground water through soil is controlled by the water pressure difference. This is true in case of flow in the horizontal direction. Figure 1.40 illustrates the variation of water pressure indicated by height of water columns in imaginary pipes installed in ground. Note that water pressure is given by $\gamma_w \times$(height of water column). However, it should be recalled that the hydrostatic condition has no flow although pressure increases in the vertical direction (Fig. 1.41). Water flow is driven by any variation of water pressure from the hydrostatic condition. Thus, it is concluded that water flow is controlled by the change of water surface elevation along the direction of water flow. The elevation of water surface, Z, consists of the elevation at the point of pressure measurement, Z_m, and the contribution by water pressure, Z_p

$$Z = Z_m + Z_p. \tag{1.23}$$

Fig. 1.40 Variation of water pressure in direction of horizontal water flow in soil

Note that Z changes in the direction of water flow in Fig. 1.40, while it is constant in Fig. 1.41.

Figure 1.42 illustrates the significance of Darcy's law on ground water flow. The elevation, Z, is measured from a fixed level, and the distance, s, is measured along the channel of water flow. The amount of water flow, v, per unit cross section of flow is given by
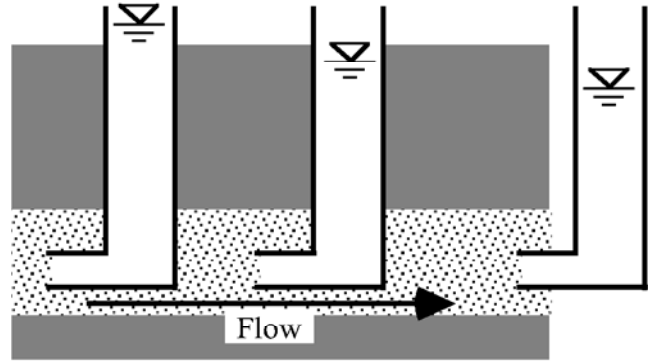
$$v = ki, \tag{1.24}$$

where the hydraulic gradient, i, is given by

$$i = \mathrm{d}Z/\mathrm{d}s. \tag{1.25}$$

The parameter of k is called the permeability coefficient, which is of the order of 0.001 to 0.01 m/s for sandy soil and less than, for example, 10^{-8} m/s for clayey soils. Note that "v" stands for the

Fig. 1.41 Distribution of water pressure in hydrostatic condition

Fig. 1.42 Definition of hydraulic gradient

amount of water flow (flux) per unit cross section per second, and is different from the velocity of water flow. The velocity is equal to $v \times (1+e)/e$ where e is the void ratio of soil (Sect. 1.2).

Since water has some viscosity, water flow exerts force in the direction of flow. Being called seepage force, this force per unit volume of soil is given by

$$\text{Seepage force} = i\gamma_w,$$

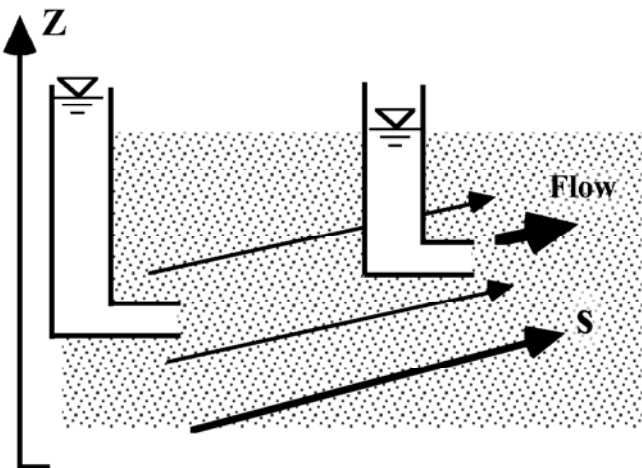where $\gamma_w (= \rho_w g)$ is the weight of water per unit volume. Figure 1.43 illustrates an extreme case in which a high rate of water flow towards the surface exerts significant force upon soil and this force is equal to the gravity force.

$$i\gamma_w = \gamma',$$

in which γ' is the buoyant weight of soil. Because of this force equilibrium, soil particles are floating in pore water and there is no effective stress any more. Consequently, soil looses shear strength (1.15). This extreme situation is called "boiling" and causes failure of earth structures such as river dike and earth dam among others. Liquefaction is another example of boiling (Sects. 18.2 and 18.3).

By using (1.1) on water saturated soil ($S_r = 1.0$),

Fig. 1.43 Hydraulic gradient at boiling

$$\gamma' = \gamma - \gamma_w = \frac{G_s - 1}{1 + e}\gamma_w \qquad \text{and}$$

$$i = i_{cr} = \frac{\gamma'}{\gamma_w} = \frac{G_s - 1}{1 + e}. \qquad (1.26)$$

When $G_s = 2.65$ and $e=0.8$ for example, the critical hydraulic gradient, i_{cr}, is approximately equal to 0.9.

📖 1.14 Shear Band

Classic soil mechanics hypothesized that shear failure and slip movement of soil occur along a plane: i.e., the boundary between stationary and moving soil masses had no thickness. Elaborate laboratory experiments in the recent times, however, found that shear failure occurs as a large shear strain that is localized (concentrated) within a narrow layer. This layer is called shear band.

Figure 1 44 demonstrates the appearance of shear band that was made visible through a transparent side wall of a special shear device. Shear failure occurred in a nearly plane-strain manner, and the movement of sand grains was recorded by a digital microscope (Furumoto et al., 1997; Towhata and Lin, 2003). Shear band developed in an oblique direction and its thickness in this postfailure photograph is approximately equal to 20 times sand grain size.

The observed shear stress–strain behavior (Fig. 1.45) shows the peak stress state that is followed by softening (decrease in stress level) and a residual state (constant stress). Note that the peak stress occurred at strain of 1.5 %.
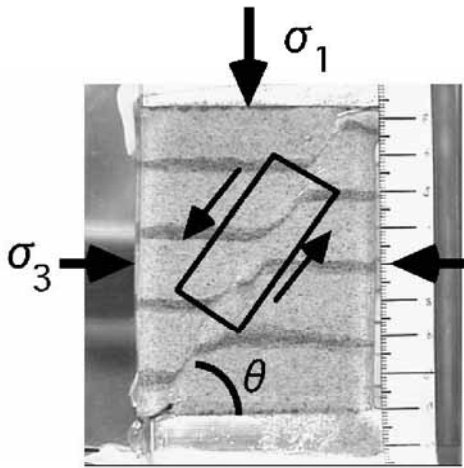
Fig. 1.44 Development of shear band in drained shear of dry Toyoura sand
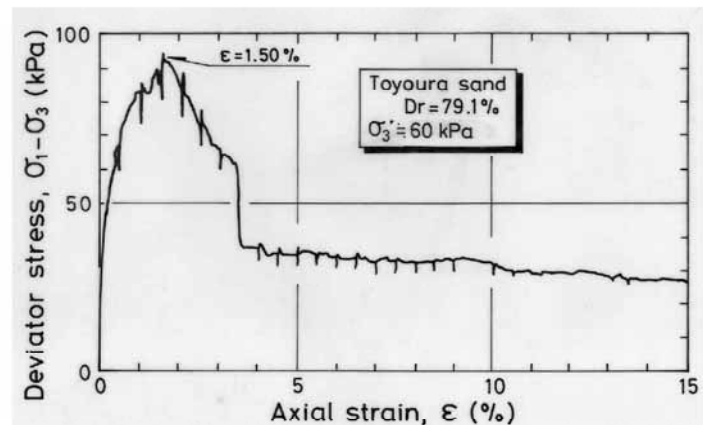
**Fig. 1.45** Stress–strain behavior of medium dense sand in transparent shear device (Dr = 79%)

The grain movement was recorded by comparing two microscopic photographs at strains of 0 % and 4 % (Fig. 1.46). This strain range includes the occurrence of the peak stress state. As shown in this figure, all the grains in the upper portion of the specimen moved together, suggesting a rigid block movement, while grains in the bottom were stationary, implying again a stable block. In contrast, the middle part indicates discontinuity in displacement due to development of shear band or strain localization in a narrow band. According to this incremental grain movement, the thickness of the shear band is less than 10 times grain size. This thickness is smaller than the aforementioned shear band thickness (Fig. 1.44) probably because the location of temporary shear band (Fig. 1.46) translates with time and induced significant dislocation of grains in a bigger area (Fig. 1.44).

The orbit of grains (Fig. 1.47) shows that the volume of grain packing increased within a shear band. This dilatant behavior leads to softening and reduced shear strength after the peak stress.

Figure 1.48 illustrates rotation of long axis of grains. It is noteworthy that significant rotation occurred within a shear band after the peak stress. Because rotational friction is lower than sliding friction, this finding may further account for the softening of stress level after the peak.

In the prepeak stage of tests, a microscopic motion picture showed that grains occasionally fall into

nearby big voids. Figure 1.49 indicates the number of grain droppings that changes with the progress of shear deformation. Since dropping disappeared after the peak strength (strain = 1.5 %), it is inferred that such dropping under increasing stress level erases large voids and improves the overall shear rigidity of sand. If this phenomenon continues for a longer time in the real subsoil, sandy ground will obtain greater rigidity and even higher liquefaction resistance. This mechanism may be a cause of ageing (Fig. 18.46) and a long-term increase in SPT-N (Fig. 26.59).
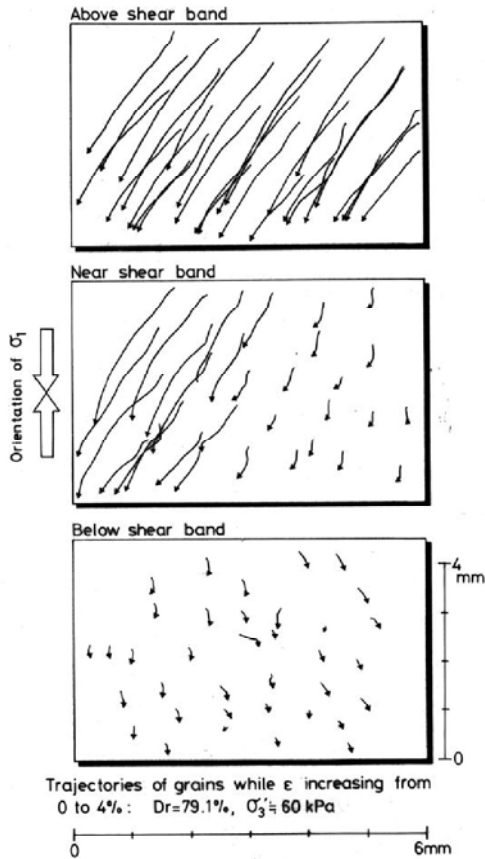
Fig. 1.46 Microscopic observation of orbit of sand grains near shear band (D_r = 79%)
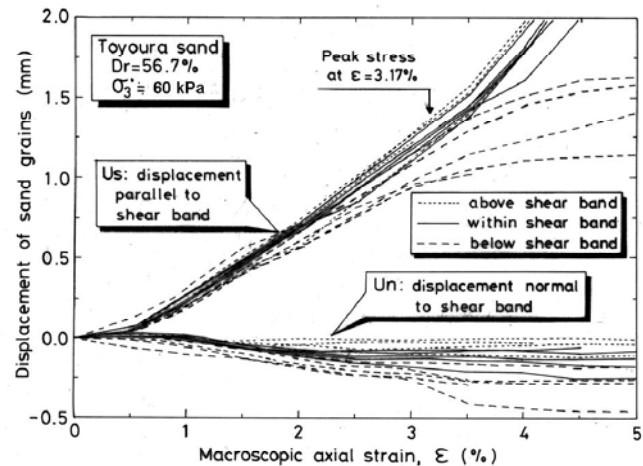
Fig. 1.47 Volume expansion in shear band (D_r = 57%)
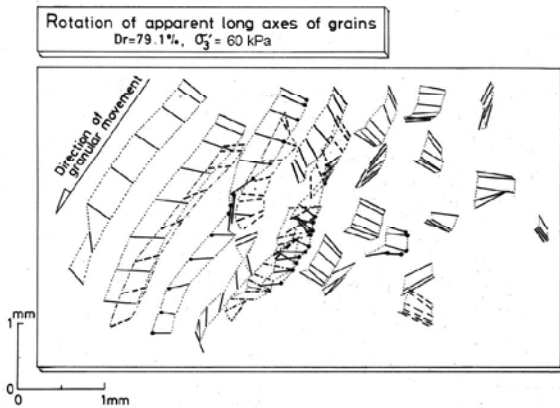
Fig. 1.48 Rotation of grains in shear band (D_r = 79%)
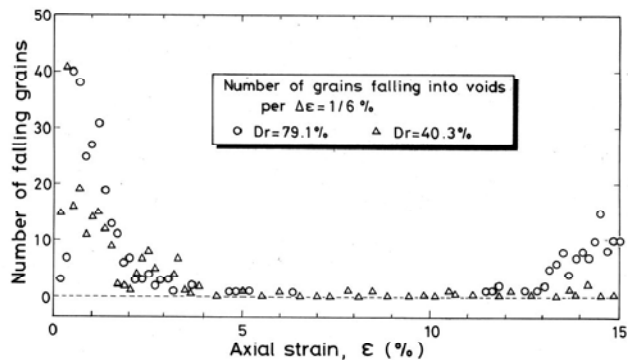
Fig. 1.49 Histogram of grains dropping into large voids

List of References in Chapter 1

Bishop, A.W. (1950) Discussion, Geotechnique, Vol. 2, No. 2, pp. 113–116.

Evans, M.D., Seed, H.B. and Seed, R.B. (1992) Membrane compliance and liquefaction of sluiced gravel specimens, J. Geotech. Eng., ASCE, Vol. 118, No. 6, pp. 856–872.

Furumoto, K., Towhata, I., and Yoshida, A. (1997) Microscopic observation of shear band in plane strain compression tests of sand, Proc. IS-Nagoya, pp. 235-240.

Japanese Geotechnical Society (2004) Mitigation measures for liquefaction, pp. 238–240 (in Japanese).

Meyerhof, G.G. (1957) Discussion of Session 1, Proc. 4th Int. Conf. Soil Mech. Found. Eng., Vol. 3, p. 110.

Newland, P.L. and Allely, B.H. (1957) Volume change in drained triaxial tests on granular materials, Geotechnique, Vol. 7, No. 1, pp. 17–34.

Nicholson, P.G., Seed, R.B. and Anwar, H.A. (1993) Elimination of membrane compliance in undrained triaxial testing, I. Measurement and evaluation, Can. Geotech. J., Vol. 30, pp. 727–738.

Raja, V.S. and Sadasivan, S.K. (1974) Membrane penetration in triaxial tests on sands, Proc. ASCE, Vol. 100, GT4, pp. 482–489.

Rowe, P.W. (1962) The stress–dilatancy relation for static equilibrium of an assembly of particles in contact, Proc. Royal Soc. Lond. A, Vol. 269, pp. 500–527.

Seed, H.B., Tokimatsu, K., Harder, L.F. and Chung, R.M. (1985) Influence of SPT procedures in soil liquefaction resistance evaluations, Proc. ASCE, Vol. 111, GT12, pp. 1425–1445.

Sivathayalan, S. and Vaid, Y.P. (1998) Truly undrained response of granular soils with no membrane-penetration effects, Can. Geotech. J., Vol. 35, No. 5, pp. 730–739.

Towhata, I., Chowdhury, F.K. and Vasantharajah, N. (1988) Cyclic undrained tests on gravel-like material using cubic triaxial apparatus, Proc. 9th World Conf. Earthq. Eng, Vol. III, pp. 53–58.

Towhata, I., Kuntiwattanakul, P., Seko, I. and Ohishi, K. (1993) Volume change of clays induced by heating as observed in consolidation tests, Soils Found., Vol. 33, No. 4, pp. 170–183.

Towhata, I., Kuntiwattanakul, P. and Kobayashi, H. (1993) A preliminary study on heating of clays to examine possible effects of temperature on soil-mechanical properties, Soils Found., Vol. 33, No. 4, pp. 184–190.

Towhata, I. and Lin, C.-E. (2003) Microscopic observation of shear behavior of granular material, Proc. IS-Lyon, Lyon.

PART 2

Problems Concerning Shaking of Soft Ground Undergoing Earthquake Loading

Statue of Buddhism at Ajanta, India.

Chapter 2

Introduction

Chan Chan archaeological site in North Peru

📁 2.1 Objectives of Earthquake Geotechnical Engineering

Earthquake geotechnical engineering is concerned with the following topics:

1. Prediction of ground motion during earthquakes
2. Prediction of residual deformation of ground and earth structures that remain after shaking
3. Study on stress–strain–strength characteristics of soils undergoing cyclic loading
4. Subsurface exploration by generating and observing propagation of ground vibration
5. Safety and/or satisfactory performance of structures during earthquakes
6. Application of knowledge to ground vibration caused by machine and traffic loading among others

In the past experiences, such earthquake-related damages as loss of human lives and properties as well as malfunctioning of facilities were induced by either a total collapse of structures or their unacceptably large deformation. Those collapse and deformation in turn were induced by either a strong shaking or a ground deformation that is not recovered after an earthquakes and remains permanently. Therefore, the topics (1) and (2) shown above are concerned with the prediction of the extent of damage.

It has been found that the ground shaking and the residual deformation that remains after shaking are strongly dependent on the stress–strain behavior of soils. Since soil is a nonlinear material, there is no proportionality between stress and strain. The deformation characteristics, and of course the strength, vary drastically with

- The magnitude of effective stress that stands for the contact forces among soil grains
- History of stress application in the past (normal or over consolidation)
- Age of soil
- Rate of loading (to some extent)
- Material strength of soil

among others. Thus, the basic understanding of soil behavior requires us to do much efforts experimentally. Consequently, many stress–strain models of soils have been proposed by a number of research people.

Even though an appropriate stress–strain model may be available for an analysis, identification of soil parameters at a specified site is further difficult. Practice runs tests in the field or collects soil specimens of good quality (this is already a big topic of study) for laboratory testing. The employed model may or may not be able to handle the complicated stress–strain behavior. The collected information may be representative of the whole ground (case of uniform ground) or indicates the behavior of a small specimen (case of heterogeneous ground).

To date, many computer codes have been developed that can calculate the earthquake shaking of ground and earth structures. They appear to be reasonable when the studied ground condition is relatively stiff. It means that the prediction is reasonable when the strain in soil is small and the nonlinearity is not significant. Conversely, computation on soft soil deposits is still difficult.

There is no general way to relate the predicted nature of ground shaking to the extent of damage. Many kinds of structures are of different causes of damages, which cannot be taken care of by a single or a limited number of seismic parameter(s).

In summary, there are still so many problems in earthquake geotechnical engineering that require further studies. It should be borne in mind that what are being discussed today at many occasions might be discarded in the next decade.

📁 2.2 Geotechnical Problems Encountered During Earthquakes

Recent earthquake events have been studied in detail and many points have been made. Consequently, it has been found that two phenomena should be studied, namely amplification of shaking and liquefaction.

1. Problems induced by shaking include the following issues:

Amplification of motion in soft alluvial deposits 軟弱沖積層における地震動の増幅
Effects of local soil conditions and topography on amplification 地盤条件や地形が地震動増幅度に及ぼす影響
Permanent (residual) deformation of earth structures 土構造物の永久変形（残留変形）
Landslide 地すべり
Different causes of seismic failure in different types of facilities 地震被害の原因は施設の種類によって異なる,
  for instance, inertia force 慣性力, deformation of surrounding soil 周辺地盤の変形, etc.
    Conventionally, earthquake engineering has been working on the intensity of acceleration 加速度 at the bottom of surface structures. This is because d'Lambert principle states the equivalence of the acceleration and the inertia force. It is, however, apparent that the acceleration does not account for the deformation/strain of the ground. Some people, therefore, prefer to use the earthquake velocity 速度 in place of acceleration for assessment of damage extent, although the physical significance of velocity is not clearly understood
Dynamic soil–structure interaction 地盤と構造物との動的相互作用
Fault movement 断層運動

2. Liquefaction causes the following problems and poses topics of study:

Effects of local geology on liquefaction potential 表層地質が液状化の可能性に及ぼす影響,
    type of soil 土の種類, age of soil 堆積後の年代
Loss of bearing capacity 支持力の喪失 and subsidence of surface structure 沈下・めり込み
Floating of embedded structure 埋設構造物の浮き上がり
Boiling of sand and water 噴砂と噴水
Consolidation and subsidence 圧密と地盤沈下
    Liquefaction is the build-up of excess pore water pressure 過剰間隙水圧 due to cyclic shear loading. When this pore pressure dissipates 消散する like consolidation of clayey deposits, the volume of sand decreases and ground subsidence 地盤沈下 occurs.
Lateral flow of ground 側方流動
    Liquefied ground flows laterally and deforms in the meantime, causing damage to many underground facilities. This is the most recent topic of study and many people are trying to demonstrate the cause of lateral flow as well as to predict the amount of flow.
Soil–structure interaction 地盤と構造物との相互作用
Prevention of liquefaction 液状化の防止
Mitigation of liquefaction-induced damage 被害の軽減
    It is still difficult to prevent liquefaction over a vast area where networks of lifelines are installed ライフライン網のような広大な施設全域で液状化を防止するのは不可能である. It is also expensive, or impossible in developed urban areas 都市域は建て込んですでに地盤を改良する余地がない. When this is the case, the bad consequences of liquefaction should be minimized by using several mitigation measures このような場合、液状化の発生はやむを得ないが、被害をなるべく少なくするような方策を考える.

📂 2.3 Schematic Diagram to Show Relationship Among Geotechnical Seismic Problems

地震断層の破壊　Rupture of fault

地震動の伝播、距離とともに減衰
Propagation of earthquake motion,
 decaying with distance

表層地盤に入射 Input in local soil

地盤で震動増幅、地盤の固有周期に共振して周波数
特性変化、地盤の自由振動で震動継続時間長期化

Amplification in surface soil, resonance at natural
period of surface layer, elongated duration of
shaking due to free vibration of surface soil

若齢の沖積または埋め立て砂質土、
ゆる詰め
Young alluvial or manmade sandy
fill, low density

液状化して地盤が泥水化
Liquefaction changes
subsoil to liquid

加速度大
Strong acceleration

動的変位が大
Large amplitude of
displacement

震動長周期化
Elongated period of
motion

重い基礎の沈下、軽い埋設物の浮上、
地盤の側方流動、圧密沈下
Subsidence of heavy foundation,
floating of light embedded
structure, lateral flow of soil,
consolidation settlement

慣性力大
Large inertial force

地盤変形が大
Large ground deformation

脆い構造物の崩壊
Collapse of less flexible and
less ductile structures

固有周期の長い構造物が共振、大振動
Resonant motion of structures
having long natural period

線状または地中構造物の過大な
変形と破壊
Unallowable distortion of linear
or embedded structures

超高層ビルの振動、液体貯蔵タンクの
揺動破壊
Oscillation of high-rise buildings,
sloshing failure of liquid storage
tanks

Chapter 3

Seismological Knowledge

Lion´s gate at Hattusas, the ruin of the capital of ancient Hittite Empire, Anatolia, Turkey.

☀ 3.1 Rupture of Fault as Cause of Earthquake

Figure 3.1 illustrates a Japanese traditional idea on causative mechanism of earthquakes. Therein a cat fish (鯰) whose movement underground caused an earthquake and destroyed present Tokyo in the middle of nineteenth century are punished by angry people. The true understanding of the cause of earthquakes started in the second half of the twentieth century.
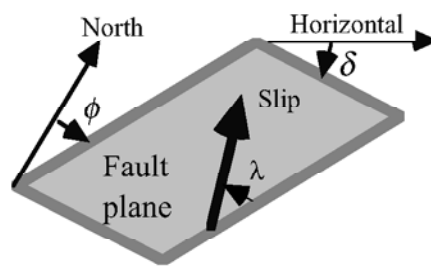
It is commonly understood today that an earthquake is caused by a rupture of a fault in the earth´s crust. Figure 3.2 shows various fault movements: normal, reverse, and (left- or right-lateral) strike-slip. The normal fault is caused by tensile stress field because the two earth blocks in Fig. 3.2 are separated from each other. In contrast, the reverse fault is generated by compressional stress field. This is the case in the subduction zone where an ocean tectonic plate subsides under a continental plate.
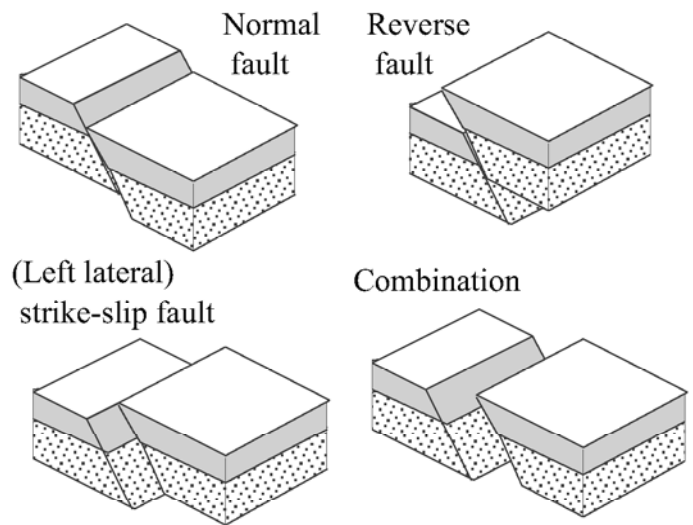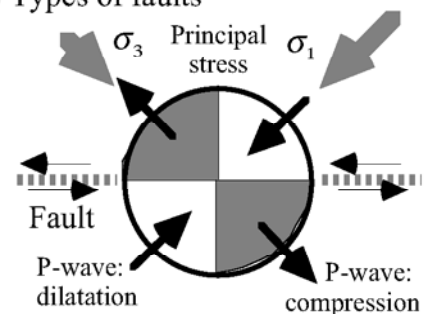
As for terminology, an earthquake hypocenter (震源) or focus stands for the place of the first rupture, whilst an epicenter (震央) is the place at the surface that lies just above the focus. See Sect. 5.10.

The geometric characteristics of a fault plane are expressed in terms of its direction (ϕ), inclination (δ), and the direction of displacement (λ) in addition to the size. Three angular information is illustrated in Fig. 3.3. Moreover, the directions of tectonic stress and fault movement are related with the direction of ground motion. Generally, the direction of the principal stress (compressional stress) is related with the direction of the first ground movement (P wave in Sect. 4.2). Thus, the observed earthquake motion is able to assess the nature of stress field and the mechanism of an earthquake causative fault. In Fig. 3.4, the white part implies the area of the first motion towards the fault (the center of fault rupture, or, more precisely, the epicenter at ground surface; see Sect. 5.10), while the shadowed part shows the first motion that is oriented away from the fault. Note that this type of diagram is in principle of a three-dimensional nature, although Figure 3.4 illustrates a simple two-dimensional situation.

The earth crust is continuously sheared or compressed by increasing tectonic forces. As the stress in rock increases with time, the strain energy is accumulated. Ultimately the crust is broken mechanically and the elastic energy is released (Fig. 3.5). Earthquake is the result. Thereafter, the accumulation of strain energy starts again towards a future earthquake.

Fig. 3.1 Stabilization of traditional earthquakes by punishing catfish

Fig. 3.2 Types of faults

Fig. 3.3 Definition of geometric parameters of fault orientation

Fig. 3.4 Example of motion in first part of P wave in strike-slip fault

The rock rupture is said to be associated with a generation of electric current. This may be related to many precursors (前兆). Measurement of electric current in Greece is making a success to some extent in prediction of earthquakes.

In reality, the whole fault does not rupture in a single event. The first breakage occurs at a place where the factor of safety is minimum. The working stress there is transferred to other portions of the fault, causing another rupture. Thus, the rupture propagates along the fault. Impact is generated from each rupture event and affects the ground surface. With all the impact combined, the ground motion is felt as an earthquake.

The number of possible earthquake occurrence in a concerned area is an important issue in assessing the regional seismic risk. Gutenberg and Richter (1944) reported a logarithmically linear relationship between seismic magnitude (M) and the number of earthquakes (n) that occurred in the California-Nevada region from 1921 to 1943

$$\log_{10} n(M) = a - bM. \qquad (3.1)$$

In this equation, $n(M)$ stands for the number of earthquakes whose magnitude lies between M–1/2 and M+1/2. Moreover, a and b are parameters that account for the local seismic activity. Since a and b were about 5 and 0.88 in their study, the above formula implies that the number of earthquakes decreases as illustrated in Fig. 3.6. Gutenberg and Richter (1944) then extended their studies to the entire world and validated the above empirical formula. Note, however, that the values of a and b parameters may vary from region to region. Moreover, a depends on the time period of concern.

The number of earthquakes, $N(M)$, whose magnitude is greater than M can be calculated by integrating (3.1);
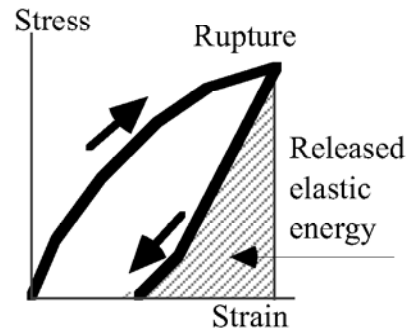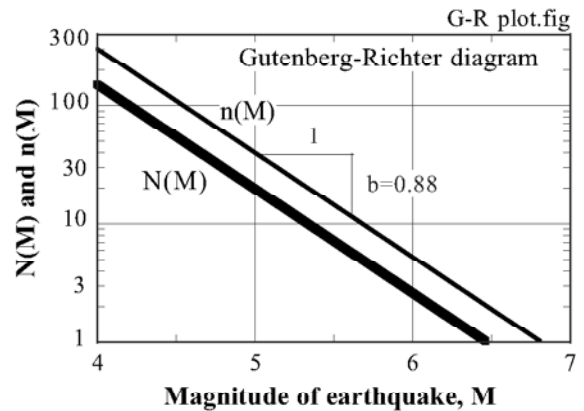
$$N(M) = \int_M^\infty n(M)\, dM.$$

Consequently,

$$\log_{10} N(M) = a - \log_{10}(b \log_e 10) - bM \qquad (3.2)$$

Fig. 3.5 Release of elastic energy after rupture

Fig. 3.6 Example illustration of Gutenberg-Richter relationship with a=5 and b=0.88

Figure 3.6 illustrates both $n(M)$ and $N(M)$ changing with M by using a=5 and b=0.88.

Recent studies in seismology reveled that the earthquake is not the only way to release the strain energy as illustrated in Fig. 3.5. The rebound may occur more slowly. This type of event is called slow earthquake, silent earthquake, or slow slip event (Kawasaki, 2006). Whatever may be the name, the rebound of the tectonic plate occurs over a long time, ranging from minutes to months, and accordingly the intensity of acceleration is very small. Noteworthy is that a slow earthquake can generate a big tsunami if the sea bed moves within a short time period. If this happens, it is possible that a disastrous tsunami attacks a coastal region despite that the associating seismic shaking is too weak to trigger any precaution.

In modern seismology (for example, Bolt, 1973), the earth's surface is divided into many plates of crust which travel laterally. Figure 3.7 attempts to show major plates that are known so far. For latest information, refer to many literatures in this field. The mechanical interaction between plates, such as collision, friction, and separation, accumulates strain and strain energy that lead ultimately to rupture. Therefore, the number of earthquakes in the plate boundary regions is significantly greater than that inside plates.
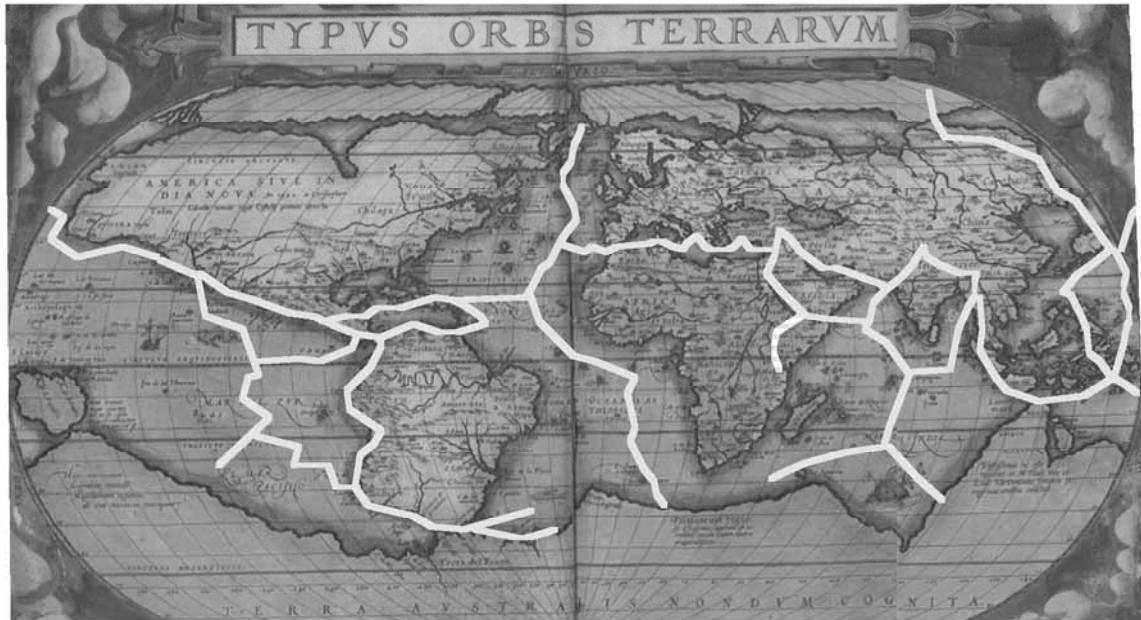
Fig. 3.7 Earth surface divided into tectonic plates
(drawn on the World Atlas by A. Ortelius, 1574: yellow lines show plate boundaries)

It is not true that all the plate boundaries generate strong earthquakes. For example, some parts of the San Andreas Fault in California, which is located along a boundary between North American and Pacific Ocean Plates, deform continuously and hence do not produce a sudden rupture. In opposition in the past, many big earthquakes occurred inside tectonic plates. A few of examples for this are the 1811–1812 New Madrid earthquake in south United States (magnitude being 8.0 or more) and the 1976 Tangshang (唐山) earthquake of magnitude=7.8 in North China. It seems that plate distortion occurs internally as well due to externally applied boundary stresses. Thus, there is virtually no earthquake-free region and the extent of earthquake risk is a matter of probability and local human population. In general, the time period until the next rupture is shorter in plate boundary earthquakes, and it is longer for internal rupture, although there are exceptions.

Separation undergoing tensile stress

Merging subject to compressive stress


Lateral slip and shear stress
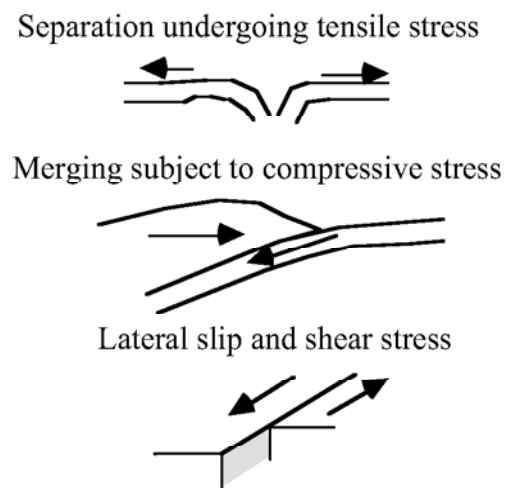
Fig. 3.8 Types of plate boundaries

Figure 3.8 illustrates three kinds of plate boundaries where two plates are being separated (e.g. the Center of the Atlantic Ocean and the Rift Valley in East Africa), merging (subduction; Himalaya, Chile, and Japan), and being subjected to shear (California).

Figure 3.9 demonstrates a causative mechanism at a subduction zone where one of the colliding plates (mostly oceanic) is sinking down into the earth. The continental plate goes up as rebound and generates an "interplate" earthquake. This earthquake usually releases a huge elastic energy. This upward rebound action may trigger tsunami in the sea water. It is possible further that the part of the continental plate behind the rebound part may subside 1 m or so, leading to inundation by sea water, Kohchi in 1946 (Sect. 16.9) and Valdivia of Chile in 1960 (Sect. 16.10).

The modern theory of plume tectonics (Maruyama, 2002) states that the plate that is going down in Fig. 3.9 melts under high temperature and pressure, reaches the core part of the earth, and finally comes back to the surface again (Fig. 3.10). This procedure takes almost one billion years.
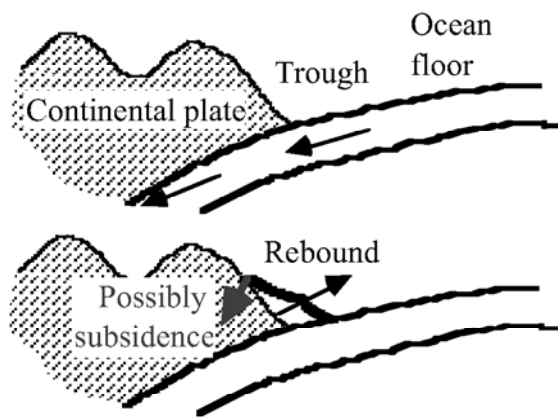
Fig. 3.9 Rupture and rebound in a
subduction zone
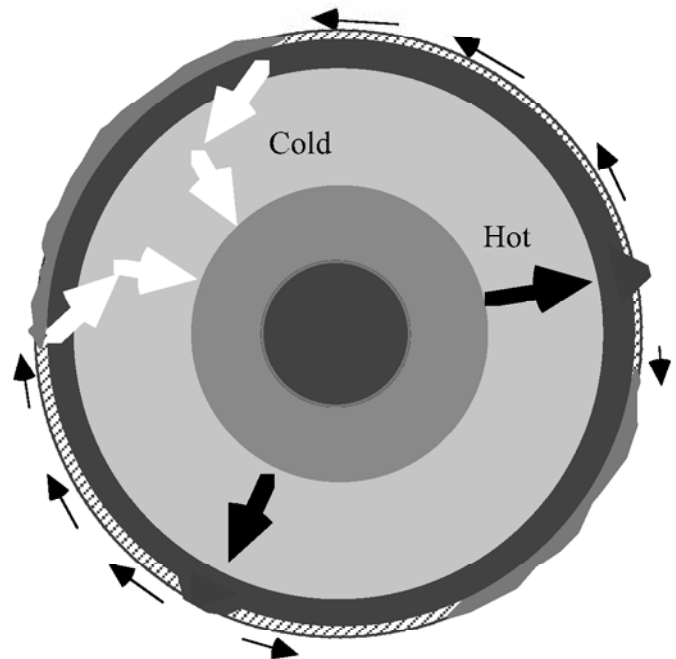
Fig. 3.10 Conceptual illustration of plume
tectonics

☀ 3.3 Reservoir-Triggered Seismicity

A unique type of earthquake triggering mechanism is found in the reservoir-triggered seismicity in which rising of water level in artificial lakes causes earthquakes. Gupta (1985) showed 44 quakes of this type among which four had magnitude greater than 6: Hsinfengkinan (M=6.0; 1962 in China), Kariba (M=6.2; 1963 in Zambia and Zimbabwe), Koyna (M=6.3; 1967 in India), and Kremasta (M=6.3; 1966 in Greece). The epicenters of reservoir-triggered earthquakes are scattered all over the world. When the Three-Gorge dam was constructed, the possibility of earthquake was discussed. Until 2007, no big earthquake has occurred in the reservoir area. It is noteworthy that the gigantic rock slide (275 million m³) at Vajont dam in Italy (1963) was preceded by

Fig. 3.11 Site of Three-Gorge Dam in China prior to construction

not only minor slope failures but also small earthquakes upon reservoir filling (Nonveiller, 1987). Gupta (1985) pointed out that the Himalaya region does not have this kind of earthquake probably because of the thrust (reverse) kind of tectonic movement. He further mentioned that some reservoir decreased the local seismicity after water impounding. Thus, much is not yet known about the mechanism of reservoir-triggered seismicity.

Simpson and Negmatullaev (1981) carried out a detailed investigation on the earthquakes in the area of Nurek reservoir in Tadjikistan, Central Asia. The Nurek dam is a 315 m high rockfill dam and formed a 40 km-long lake in one of the tributaries of the Amu Dary´a River. Figure 3.12 shows that earthquakes were induced when the reservoir level achieved new maximums. It was pointed out further that the very rapid draw-down of water level in early 1975 induced earthquakes. Thus, the reservoir-triggered earthquake is somehow related with the overburden pressure and pore pressure, which takes some time to propagate into rock mass and affects the rock stability. It was of further interest that the epicenters of the earthquakes migrated from the downstream area to the upstream area around the reservoir. This infers that seismicity is ceased when the strain energy is released and the earthquakes occurs in the newly impounded upstream area.
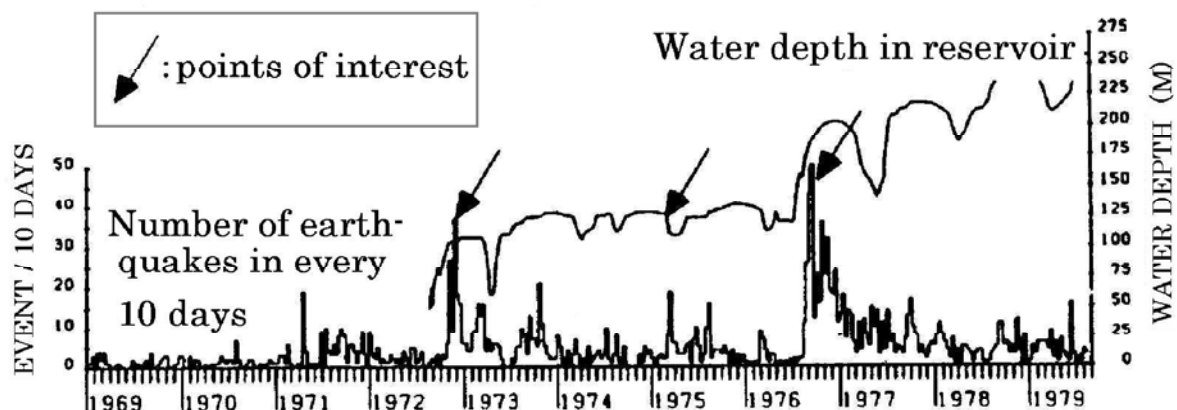
Fig. 3.12 Correlation between number of earthquake events per 10 days and reservoir water depth at Nurek (Simpson and Negmatullaev, 1981)

List of References in Chapter 3

Bolt, B.A. (1973) Earthquakes and Geological Discovery, Scientific American Library, ISBN 0-7167-5040-6.

Gupta, H.K. (1985) The present status of reservoir induced seismicity investigations with special emphasis on earthquakes, Tectonophysics, Vol. 118, pp. 257–279.

Gutenberg, B. and Richter, C.F. (1944) Frequency of earthquakes in California, Bull. Seismol. Soc. Am., Vol. 34, pp. 185–188.

Kawasaki, K. (2006) Introduction to slow earthquake, NHK Books 1005, ISBN 4-14-091055-0 C1344 (in Japanese).

Maruyama, S. (2002) Evolution of earth, Decoding the earth's evolution, Ed., Kumazawa, M., Ito, T. and Yoshida, S., University of Tokyo Press, ISBN 4-13-060741-3, pp. 18–54 (in Japanese).

Nonveiller, E. (1987) The Vajont reservoir slope failure, Eng. Geol., Vol. 24, p. 499.

Simpson, D.W. and Nagmatullaev, S.K. (1981) Induced seismicity at Nurek reservoir, Tadjikistan, USSR, Bull. Seismol. Soc. Am., Vol. 71, No. 5, pp. 1561–1586.